Neurobiology of Disease 181 (2023) 106106

Contents lists available at ScienceDirect

Neurobiology of Disease

journal homepage: www.elsevier.com/locate/ynbdi

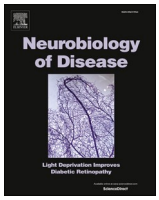

Lamotrigine rescues neuronal alterations and prevents seizure-induced memory decline in an Alzheimer's disease mouse model

Emanuela Rizzello [a,1], Domenico Pimpinella [a,1], Annabella Pignataro [b,c], Giulia Titta [a], Elisabetta Merenda [a], Michela Saviana [b], Giovanni Francesco Porcheddu [a], Chiara Paolantoni [a], Francesca Malerba [a], Corinna Giorgi [a,d], Giulia Curia [e,***], Silvia Middei [a,f,**], Cristina Marchetti [a,d,*]

[a] European Brain Research Institute (EBRI)- Fondazione Rita Levi-Montalcini, Rome, Italy
[b] Laboratory of Psychobiology, Department of Experimental Neurology, Santa Lucia Foundation, Rome, Italy
[c] National Research Council (CNR)- Institute of Translational Pharmacology (IFT), Rome, Italy
[d] National Research Council (CNR)- Institute of Molecular Biology and Pathology (IBPM), Rome, Italy
[e] Dipartimento di Scienze Biomediche, Metaboliche e Neuroscienze, e Centro di Neuroscienze e Neurotecnologie, Università degli Studi di Modena e Reggio Emilia, Modena, Italy
[f] National Research Council (CNR)-Istituto di Biochimica e Biologia Cellulare (IBBC), Monterotondo, Italy

ARTICLE INFO

Keywords:
Alzheimer's disease
hippocampus
Epilepsy
Neuronal excitability
Contextual fear conditioning
Lamotrigine

ABSTRACT

Epilepsy is a comorbidity associated with Alzheimer's disease (AD), often starting many years earlier than memory decline. Investigating this association in the early pre-symptomatic stages of AD can unveil new mechanisms of the pathology as well as guide the use of antiepileptic drugs to prevent or delay hyperexcitability-related pathological effects of AD. We investigated the impact of repeated seizures on hippocampal memory and amyloid-β (Aβ) load in pre-symptomatic Tg2576 mice, a transgenic model of AD. Seizure induction caused memory deficits and an increase in oligomeric $A\beta_{42}$ and fibrillary species selectively in pre-symptomatic transgenic mice, and not in their wildtype littermates. Electrophysiological patch-clamp recordings in *ex vivo* CA1 pyramidal neurons and immunoblots were carried out to investigate the neuronal alterations associated with the behavioral outcomes of Tg2576 mice. CA1 pyramidal neurons exhibited increased intrinsic excitability and lower hyperpolarization-activated I_h current. CA1 also displayed lower expression of the hyperpolarization-activated cyclic nucleotide-gated HCN1 subunit, a protein already identified as downregulated in the AD human proteome. The antiepileptic drug lamotrigine restored electrophysiological alterations and prevented both memory deficits and the increase in extracellular Aβ induced by seizures. Thus our study provides evidence of pre-symptomatic hippocampal neuronal alterations leading to hyperexcitability and associated with both higher susceptibility to seizures and to AD-specific seizure-induced memory impairment. Our findings also provide a basis for the use of the antiepileptic drug lamotrigine as a way to counteract acceleration of AD induced by seizures in the early phases of the pathology.

Abbreviations: Aβ, Amyloid-β; ACSF, Artificial cerebrospinal fluid; AD, Alzheimer's Disease; ADP, Afterdepolarization; AED, Antiepileptic Drug; aMCI, amnestic Mild Cognitive Impairment; APP, Amyloid precursor protein; CFC, Contextual Fear Conditioning; DMSO, Dimethyl sulfoxide; ES, Electroshock; fAHP, fast afterhyperpolarization; FFT, Fast Fourier Transform; HCN, Hyperpolarization-activated cyclic nucleotide-gated channels; I_h, Hyperpolarization-activated current; i.p., intraperitoneal; LTG, Lamotrigine; mAHP, medium afterhyperpolarization; OC, fibrillar oligomers; qRT-PCR, quantitative RT-PCR; R_{in}, Input Resistance; RMP, Resting Membrane Potential; RT-PCR, Real-Time PCR; TBS, Tris-buffered saline; TBST, TBS with Tween; Tg, Tg2576; VEH, Vehicle; Wt, Wild-type; ZAP, Impedance (Z) amplitude profile.

* Correspondence to: C. Marchetti, National Research Council (CNR)-Institute of Molecular Biology and Pathology (IBPM), Piazzale Aldo Moro 5, 00185 Rome, Italy.

** Correspondence to: S. Middei, National Research Council (CNR)-Istituto di Biochimica e Biologia Cellulare (IBBC), Via E. Ramarini, 32, 00015 Monterotondo Scalo Roma Monterotondo, Italy.

*** Correspondence to: G. Curia, Università di Modena e Reggio Emilia, Dipartimento di Scienze Biomediche, Metaboliche e Neuroscienze, Via G. Campi, 287 – 41125 Modena, Italy.

E-mail addresses: giulia.curia@unimore.it (G. Curia), silvia.middei@cnr.it (S. Middei), cristina.marchetti@cnr.it, c.marchetti@ebri.it (C. Marchetti).

[1] These authors contributed equally to this work.

https://doi.org/10.1016/j.nbd.2023.106106
Received 10 February 2023; Received in revised form 17 March 2023; Accepted 25 March 2023
Available online 29 March 2023

1. Introduction

Epilepsy is a significant comorbidity of Alzheimer's disease (AD), that correlates with earlier onset and faster progression of cognitive decline (Baker et al., 2019; Giorgi et al., 2020; Vossel et al., 2017, 2013). Contrary to other morbidities, in AD seizures occur more frequently in younger subjects and in the early-onset population (Vossel et al., 2017), suggesting that they are not simply a consequence of the advanced stages of the pathology.

Individuals carrying genetic AD mutations or at high risk for developing the disease can be followed in the phases leading to cognitive decline. In these individuals, functional magnetic resonance imaging studies show that decades before the clinical onset, brain circuits supporting cognition and involved in AD exhibit altered activity, including network activation and deactivation deficits and hippocampal hyperactivation (reviewed in Palop and Mucke, 2016). *In vivo* electroencephalography (EEG) studies in transgenic mouse models of AD have also shown that abnormal brain oscillatory activity and circuit hypersynchrony are detected before the onset of cognitive deficits (Bezzina et al., 2015; Kam et al., 2016; Palop and Mucke, 2016). The above observations prompt the question of whether early Alzheimer's disease and epilepsy share specific pathogenic mechanisms. Their understanding could provide new insights into the pre-clinical alterations of AD and could lead to a better outcome of pharmacological treatment of epilepsy, thus reducing the burden of the pathology.

The use of antiepileptic drugs (AEDs) in AD has been explored in several clinical investigations (Bakker et al., 2012; Cumbo and Ligori, 2010; Vossel et al., 2013). Among the different drugs tried, levetiracetam and lamotrigine (LTG) were more efficient in controlling seizures and led to a better outcome of cognitive performance (reviewed in Vossel et al., 2017; Toniolo et al., 2020). Yet the mechanisms through which AEDs ameliorate cognition have not been fully elucidated.

Studies in transgenic animal models of AD have revealed electrophysiological alterations in the hippocampus, which might correlate to hyperexcitability of this brain region (Alcantara-Gonzalez et al., 2021; Brown et al., 2011; Kerrigan et al., 2014; Kim et al., 2021; Šišková et al., 2014; Tamagnini et al., 2015; Verret et al., 2012; Wykes et al., 2012). These studies were mostly conducted at symptomatic ages, but exploring epilepsy-related cellular alterations in pre-symptomatic AD could potentially uncover unknown mechanisms underlying the emergence of the disease.

In this study, we took advantage of the link between epileptic seizures and cognitive decline in AD to gain understanding of the cellular alterations that underlie the early phases of the pathology. To this end, we used 1–2 months old Tg2576 mice (expressing the human APP*Swe* KM670/671NL mutation), which display intact hippocampal glutamatergic transmission and contextual memory (D'Amelio et al., 2011; Rizzello et al., 2020), but already exhibit spontaneous interictal spikes, higher susceptibility and higher mortality in response to chemically and audiogenic induced seizures (Bezzina et al., 2015; Kam et al., 2016; Kazim et al., 2021; Szabo et al., 2023; Westmark et al., 2010). Thus, we assessed seizure susceptibility with an electroshock (ES) protocol and tested whether recurrent seizures play a role in inducing memory deficits in pre-symptomatic AD mice. We then examined hippocampal neuronal properties that might correlate to higher seizure susceptibility. Our electrophysiology and molecular data point to an involvement of hyperpolarization-activated cyclic nucleotide-gated (HCN) channels, which are among the targets of the AED lamotrigine (LTG). Thus, we tested whether LTG could rescue the alterations observed at both the cellular and behavioral level. Our findings support the use of lamotrigine to counteract acceleration of AD induced by seizures in the early phases of the pathology.

2. Materials and methods

2.1. Animals

Heterozygous Tg2576 mice, expressing the human amyloid precursor protein (APP) Swedish KM670/671NL mutation (APP*Swe*) (Hsiao et al., 1996) on a C57BL/6/SJL genetic background, and wild-type (Wt) littermates were used at 1–2 months of age. Experiments were performed in accordance to the ARRIVE guidelines, the European Committee Council Directive 2010/63 and the Italian Animal Welfare legislation (D.L. 26/2014). They were approved by the Italian Ministry of Health and by the EBRI Animal Welfare Body. All efforts were made to minimize animal suffering and to reduce the number of animals used. Animals were housed under standard controlled laboratory conditions with a 12 h light/dark cycle and free access to food and water. During *in vivo* experiments (seizures and LTG treatment), animal weight was constantly monitored. In all experiments, littermates were randomly assigned to each experimental group. Suppl. Fig. 1 contains a schematic with the groups used for each experiment, including number of animals and sex.

2.2. Detection of spontaneous seizures in 1.5 month old mice

Seizures in AD mouse models are characterized by motor manifestations (Kam et al., 2016; Minkeviciene et al., 2009). In particular, Tg2576 mice at 7–8 months show severe convulsive seizures (Kam et al., 2016). Thus, to investigate whether Tg2576 mice and their Wt littermates exhibit spontaneous seizures at the age of our experiments, continuous 24-h long video-recordings were performed starting at 1.5 months for 14 days. Videos were analyzed according to the Racine scale (Racine, 1972). No seizures were detected in either the Tg2576 ($n = 11$) or the Wt ($n = 8$) group.

2.3. Electroshock (ES) protocol

A repeated ES protocol was used to induce multiple, controlled, epileptic seizures over several days. Specifically, Tg2576 and Wt littermates received five sessions of ES (Cardoso et al., 2009; Mareš and Kubová, 2006), starting at 1.5 months of age. Sessions were carried out at 10 am once every 3 days, for a total of 13 days. For ES stimulation, mice (named ES-Wt and ES-Tg2576, respectively) were placed in a transparent plexiglass cage. Stimuli (1 ms, 100 Hz, for 1 s) were delivered via silver ear-clip electrodes connected to a stimulus generator (ECT Unit 57800, Ugo Basile, Italy). The intensity of stimulation ranged from 5 to 25 mA. During stimulation, ear-clips were held by the experimenter and released immediately afterwards. Electrical conductance of clip-to-ear contact was increased with a drop of sodium chloride (0.9%) solution.

2.4. Electroshock (ES) seizure score and intensity of stimulation

Mice were recorded for at least 3 min with a video camera connected to a computer and their behavior was analyzed offline. The severity of seizures during the ES session was graded according to the following modified Racine scale (Mareš and Kubová, 2006): 0: no response; 1: facial spasms; 2: wild running; 3: Straub tail, clonus; 4: tonic-clonic seizure with upright posture; 5: tonic-clonic seizure with loss of upright posture. If mice lost the upright posture for >1 min, an extra point was added for every minute spent lying down (2 points maximum, thus the score range for each episode was 0–7 points). The total seizure score was calculated as the sum of points from each session.

Seizures induced with a strong current were sometimes characterized by a particularly pronounced tonic component that lead to death of the animal. The mortality rate for Wt and Tg2576 mice was evaluated in a first cohort of animals and is reported in the Results section, together with the intensity of stimulation. For subsequent experiments (i.e. the

ones where contextual fear conditioning or Aβ levels were evaluated after the ES protocol), the intensity of stimulation was set as follows: during the first session all animals received 10 mA (or 12 mA, if treated with LTG). At each subsequent session, based on the ES score, the intensity was changed (usually ±2 mA) with the aim of achieving the same final ES score. All animals had at least one epileptic seizure with score ≥ 5. In order to evaluate the appearance of convulsive status epilepticus, mice were monitored for 2 h after each ES session; in addition, they were monitored daily for at least one hour. In line with previous reports (Cardoso et al., 2009), convulsive status epilepticus was never observed in these mice. ShamES mice were brought into the experimental room, placed in the plexiglass cage with ear-clips attached, but did not receive the shock.

2.5. Contextual fear conditioning (CFC)

Starting 5 days before the CFC experiment, mice were handled for 5 min every day by the same experimenter who performed the CFC procedure. Experiments were carried out in two different CFC chambers, a TSE apparatus (23 × 23 × 35 cm, TSE Systems) or a Fear Conditioning Systems Series 46,001 (17 × 17 × 25 cm, Ugo Basile). In both cases, the protocol was as following. For the training session, the mouse was placed in the conditioning chamber for 120 s of free exploration, followed by a series of five non-signaled foot shocks (0.7 mA, 2 s duration, separated by 60 s intervals) delivered through the grid floor. One minute after the delivery of the fifth foot shock, mice were returned to their home cage. CFC was assessed 24 h later by placing the mouse back in the conditioning chamber for 5 min, with no foot shock (CFC test). Fear memory was estimated by recording the time the mouse spent freezing, identified as mouse immobility with the exception of respiratory movements. Mouse behavior was recorded with a video camera connected to a computer equipped with dedicated software (Noldus Ethovision, The Netherlands, and ANY-maze, UK, respectively). In order to ensure that analysis from the two systems was homogeneous, immobility was manually assessed by an experimenter blind to the experimental condition and confirmed by automatic measurements performed through the Noldus or ANY-maze software (immobility threshold set at 95%). Data are presented as the percentage of time the mouse spent freezing in the 5 min test session.

2.6. In vivo LTG treatment

Tg2576 mice received an intraperitoneal (i.p.) injection of LTG (10 mg/kg, Abcam, UK) or vehicle (VEH) every day at 9 am. Injections started 8 days before the first ES session (i.e. around P38) and lasted for the whole duration of the ES (13 days) and CFC (2 days) protocols (23 days total). LTG was dissolved in dimethyl sulfoxide (DMSO, Sigma-Aldrich) at a concentration of 20 mM and stored in aliquots at −20 °C. On the day of the injection, an aliquot was thawed and dissolved in saline (0.9% NaCl) to achieve a final dilution of 10%. VEH solution was made with the same 10% dilution of DMSO in saline. Site of i.p. injection for each mouse was alternated between the right and left side.

2.7. Electrophysiology recordings in ex-vivo slices

Acute slices were obtained from 1 to 2 months old Tg2576 and Wt mice. Animals were anesthetized with isoflurane (1-chloro-2,2,2-trifluoroethyl difluoromethyl ether) and decapitated. Coronal brain slices including the hippocampus (300 μm thick, Bregma −1.94 to −2.06 mm) were prepared with a vibratome (Leica VT1200S) in cold high sucrose solution containing (in mM): 234 sucrose, 11 glucose, 24 $NaHCO_3$, 2.5 KCl, 1.25 NaH_2PO_4, 10 $MgSO_4$, and 0.5 $CaCl_2$, saturated with 95% O_2 and 5% CO_2. Slices were then kept in artificial cerebrospinal fluid (ACSF) at 35 °C for 1 h, and subsequently at room temperature. ACSF had the following composition (in mM): 126 NaCl, 26 $NaHCO_3$, 2.5 KCl, 1.25 NaH_2PO_4, 2 $MgSO_4$, 2 $CaCl_2$, and 10 glucose (pH 7.3, saturated with 95% O_2 and 5% CO_2). For recordings, slices were transferred to an upright microscope (Nikon Eclipse E600FN) and constantly perfused with ACSF at 32 ± 1 °C. CA1 pyramidal cells were visually identified and recorded with the patch-clamp technique in the whole-cell current clamp configuration. Electrodes (tip resistance = 3–4 MΩ) were filled with an intracellular solution containing (in mM): 130 K-gluconate, 10 KCl, 10 HEPES, 1 EGTA, 2 $MgCl_2$, 4 Mg_2ATP, 0.3 NaGTP, pH = 7.3 and osmolarity ~290 mOsm. Signals were amplified using a Multiclamp 700B patch-clamp amplifier (Molecular Devices, USA), filtered at 10 kHz and sampled at 20 kHz, with a Digidata 1440 (Molecular Devices, USA). The series resistance (Rs) of neurons was continuously monitored. Cells were discarded if Rs > 20 MΩ, if Rs changed >15% from the initial values, or if the resting membrane potential was more depolarized than −55 mV. A maximum of 2 cells per slice and 3 cells per animal were used for each group. Data acquisition and analysis were performed with pClamp 10 (Molecular Devices, USA), Origin 8 (OriginLab Corporation, USA) and Prism 8 (GraphPad, USA) softwares.

An input-output curve with the number of spikes versus input current was obtained by injecting positive current steps of 1 s duration: each step had a constant current intensity in a range between +50 and + 700 pA, with increments of +50 pA. Current steps lasting 600 ms, in the range −60 to +60 pA with 20 pA increments were injected to the cell to measure input resistance (R_{in}). Membrane voltage deflection was measured at steady-state, and the resistance value calculated according to Ohm's law from the slope of the current-voltage (I-V) relationship. *Rheobase* current, defined as the minimal current intensity needed to evoke at least one spike, was measured from positive current steps between +20 and + 200 pA, with increments of +20 pA. Spikes that were at least 80 ms apart were used to measure the following parameters: spike threshold (mV), amplitude (mV), half-width (ms), rise and decay slopes (mV/ms). Action potential threshold was calculated as the voltage value corresponding to 4% of max dV/dt (Khaliq and Bean, 2010). Action potential amplitude was calculated as the difference between the threshold and the maximum height of the spike; the half-width was measured as the duration of the action potential at 50% of its amplitude. Rise and decay slopes were calculated between 20% and 80% of the action potential amplitude.

The amplitude of the fast and medium hyperpolarizations (fAHP and mAHP, in mV) were measured from threshold. Fast AHP latency was calculated as the time interval between the maximum voltage reached by the action potential and the fAHP negative peak. After the fAHP, CA1 pyramidal neurons exhibit afterdepolarization (ADP), the size of which was measured from the baseline of the action potential as the integrated area (mV·ms) under the curve between the fAHP and 10 ms after (Metz et al., 2007).

The contribution of the hyperpolarization-activated current (I_h) was evaluated through its characteristic sag in response to hyperpolarizing current injections (600 ms, from −50 pA to −200 pA). The sag was calculated as $100 \cdot (1 - V_{ss}/V_{peak})$, where V_{ss} is the value of the membrane potential (mV) at the steady-state and V_{peak} is the amplitude (mV) from the baseline of the most negative point of the trace. The post-inhibitory rebound peak, i.e. the positive peak at the end of the hyperpolarizing step, was measured with respect to the baseline voltage, i.e. before the negative step was delivered.

The impedance (Z) amplitude profile (ZAP) method was used to evaluate the electrical resonance behavior of CA1 pyramidal cells. During whole cell current-clamp recordings, a sinusoidal current (the ZAP current) was injected at a holding potential of −70 mV. The ZAP current had a constant amplitude (20–80 pA, depending on cell resistance) with linearly increasing frequency (0–15 Hz for 30 s) eliciting the voltage response. Resonance was detectable as a distinct and reproducible peak in the voltage response corresponding to a certain

frequency. The impedance profile (the relationship between the voltage response and the input current as a function of the frequency) was calculated by dividing the fast Fourier transform (FFT) of the voltage response by the FFT of the input ZAP current. The frequency at which the impedance amplitude reached its maximum was the resonance frequency. The power was calculated as the impedance at the resonance peak.

2.8. Protein extraction, native dot blot and western blot analysis for amyloid-β (Aβ) and APP

Mice (either naïve homecage, ShamES or euthanized one hour after the last ES session) were sacrificed by cervical dislocation and hippocampal samples were immediately dissected out and collected on ice. Samples were then homogenized in Tris-buffered saline (TBS: 20 mM Tris HCl, 150 mM NaCl, pH 7.4, *v/w* 2:1) and ultra-centrifuged using TLA 100.4 Rotor (Beckman Coulter) for 60 min at 65000 r.p.m. and 4 °C. The supernatant (TBS extract) was collected and stored at −80 °C. A Bradford assay was used to determine protein concentration. Native dot blot analyses were performed as in Pignataro et al. (Pignataro et al., 2019) with antibodies directed against the C-terminal of $A\beta_{42}$ (clone 295F2) or fibrillar oligomers (OC). The C-terminal-specific anti-$A\beta_{42}$ antibody (clone 295F2) selectively detects $A\beta_{42}$ but no other Aβ/APP-truncated forms while the OC antibody detects fibrillar oligomers. Homogenates (150 ng) from TBS extracts were spotted on a 0.22 μm nitrocellulose membrane. Membranes were allowed to air dry and were subsequently blocked in 5% non-fat dry milk in TBST buffer (0.1% Tween 20 in Tris–borate saline). Membranes were then incubated with $A\beta_{42}$ (295F2, Synaptic System, diluted 1:1000), OC (Merk Millipore, diluted 1:1000), or α-tubulin (Sigma, diluted 1:5000) antibodies overnight at 4 °C. After two 10-min washes in TBS and one 10-min wash in TBST, membranes were incubated with the appropriate horseradish peroxidase-conjugated (HRP)-conjugated secondary antibodies (Cell Signaling, diluted 1:5000) for 2 h. Dot blots were developed by iBright CL1000 (Thermo Fisher) and quantified with ImageJ (https://imagej.nih.gov/ij/). Each optical density signal was normalized to its α-tubulin control. Within one experiment, values were expressed as fold-change with respect to the control condition (ShamES or naïve group). Each experiment was then repeated (technical duplicate) and the two measures from the same animal (fold-change with respect to its control) were averaged to give the final value reported. In the figures, each sample (dot) corresponds to a different experimental mouse.

Western blots against APP were performed with the 22C11 antibody, which recognizes amino acids 66–81 of the N-terminus. Homogenates from the TBS fraction containing 50 μg of total protein were separated in a 4–15% sodium dodecyl sulfate–polyacrylamide pre-casted gel (Biorad, USA) and transferred to nitrocellulose membranes (Biorad, USA). Membranes were blocked in 5% non-fat dry milk in TBST buffer then incubated with the primary antibodies (22C11 and α-tubulin) overnight at 4 °C. Membranes were then washed three times for 10 min and incubated with the appropriate HRP-conjugated secondary antibodies (Cell Signaling, diluted 1:5000) for 2 h. Western blots were developed by iBright CL1000 (Thermo Fisher) and quantified with ImageJ (https://imagej.nih.gov/ij/). α-tubulin was used as normalizing control.

2.9. Western blotting and real-time (RT)-PCR for HCN channel mRNA and protein quantification

Tg2576 and Wt mice were deeply anesthetized with isoflurane (1-chloro-2,2,2-trifluoroethyl difluoromethyl ether) before decapitation. The brain was extracted and hardened at low temperatures, and ~ 900 μm thick slices were obtained. The CA1 area was then isolated with a scalpel and subjected to protein and RNA extraction. Total lysates were obtained by homogenizing each CA1 tissue in RIPA buffer (20 mM Tris-HCl pH 7.6, 150 mM NaCl, 2 mM EDTA, 1% NP-40) and incubating on ice for 30 min. Half of the lysate was processed for RNA extraction, as detailed below, and the remaining half utilized for protein isolation and Western blotting as follows. Total protein lysates were cleared by centrifugation at 10.000 x*g* for 10 min and total protein concentration of the cleared supernatant was measured by absorbance reading at A 280 (Nanodrop spectrophotometer). Equal amounts (30 μg) of each sample were separated on a 8% SDS-PAGE gel and resolved proteins were transferred onto a nitrocellulose membrane overnight in Tris-glycine buffer with 15% methanol. Homogeneous transfer was verified by Ponceau staining. Upon saturation of the membrane with TBST milk (10 mM Tris, pH 8.0, 150 mM NaCl, 0.5% Tween 20, 5% nonfat milk), incubation with primary antibodies was carried out overnight in TBST milk. Primary antibodies used were: anti-HCN1 (goat polyclonal HCN1 (V-17): sc-19,706 Santa Cruz Biotechnology; dilution 1:200); anti β-actin (mouse monoclonal 1:5000 Sigma Aldrich). Membranes were subsequently washed three times for 10 min and incubated with a 1:5000 dilution of HRP secondary antibody (HRP anti-goat, Santa Cruz; HRP anti-mouse, Chemicon) for 1 h. Blots were finally washed three times with TBST and developed with the ECL system (Amersham Biosciences) according to the manufacturer's protocols. Using ImageJ software, intensity levels detected for HCN1 were normalized against β-actin levels from the same sample. Normalized values were then utilized to quantify differences in expression between genotypes.

RNA extraction and quantitative RT-PCR (qRT-PCR) were performed as follows. Total CA1 lysates were incubated with 1 ml TRIzol Reagent (Invitrogen) and RNAs extracted following manufacturer's protocol. Extracted RNAs were resuspended in 30 μl of RNase-free H_2O, treated with DNase I (Promega), extracted again with phenol/chloroform and precipitated with ethanol and glycogen. RNAs were finally resuspended in 30 μl of RNase-free H_2O and utilized as template for one-step qRT-PCR using the GoTaq 1-Step RT-qPCR System (Promega) following the manufacturer's instructions. Primer pairs utilized were as follows: mouse HCN1 mRNA (forward: CGACTCGATCGGATAGGCAA; reverse: TGCAGTTGAGGGCTGTCATT), mouse GAPDH mRNA (forward: AACTTTGGCATTGTGGAAGG; reverse: ACACATTGGGGGTAGGAACA). qRT-PCR was performed on an iCycler iQ5 Real-Time Detection system (Bio-Rad, USA). For quantification, the ΔΔCt method was used to calculate relative HCN1 mRNA fold changes normalized against GAPDH mRNA. Each sample was analyzed in triplicate and repeated in two independent qRT-PCR experiments.

2.10. Statistical analysis

Results in the text are presented as mean ± SEM. For behavior and dot blot experiments, n refers to the number of animals used. For electrophysiology experiments, n refers to the number of cells; the number of animals from which the cells come is indicated in the figure legends. A Shapiro-Wilk normality test was carried out on all datasets to check for Gaussian distribution of the data. Normally distributed data were analyzed with a two-tailed *t*-test (paired or unpaired) or an ANOVA, depending on the number of groups compared. Statistical comparison of non-normally distributed data was performed with the Mann-Whitney *U* test for unpaired data and the Wilcoxon signed rank test for paired data. Post-hoc analysis was carried out with a Sidak's multiple comparison test, according to the software recommendation (GraphPad Prism 8). Analysis of mouse survival rate for ES experiments (Suppl. Fig. 2D) and analysis on percentages (Fig. 4B) were performed with the Fisher's exact test. For dot blot experiments, an a priori power analysis was performed with preliminary results having $n = 3$ samples (=3 male mice) per group. In all cases, Cohen's sample size (d) was "very large" (Fig. 1G: d = 3.1, Fig. 1H: d = 3.7, Fig. 5F: d = 1.15, Fig. 5G: d = 1.42) and determined a

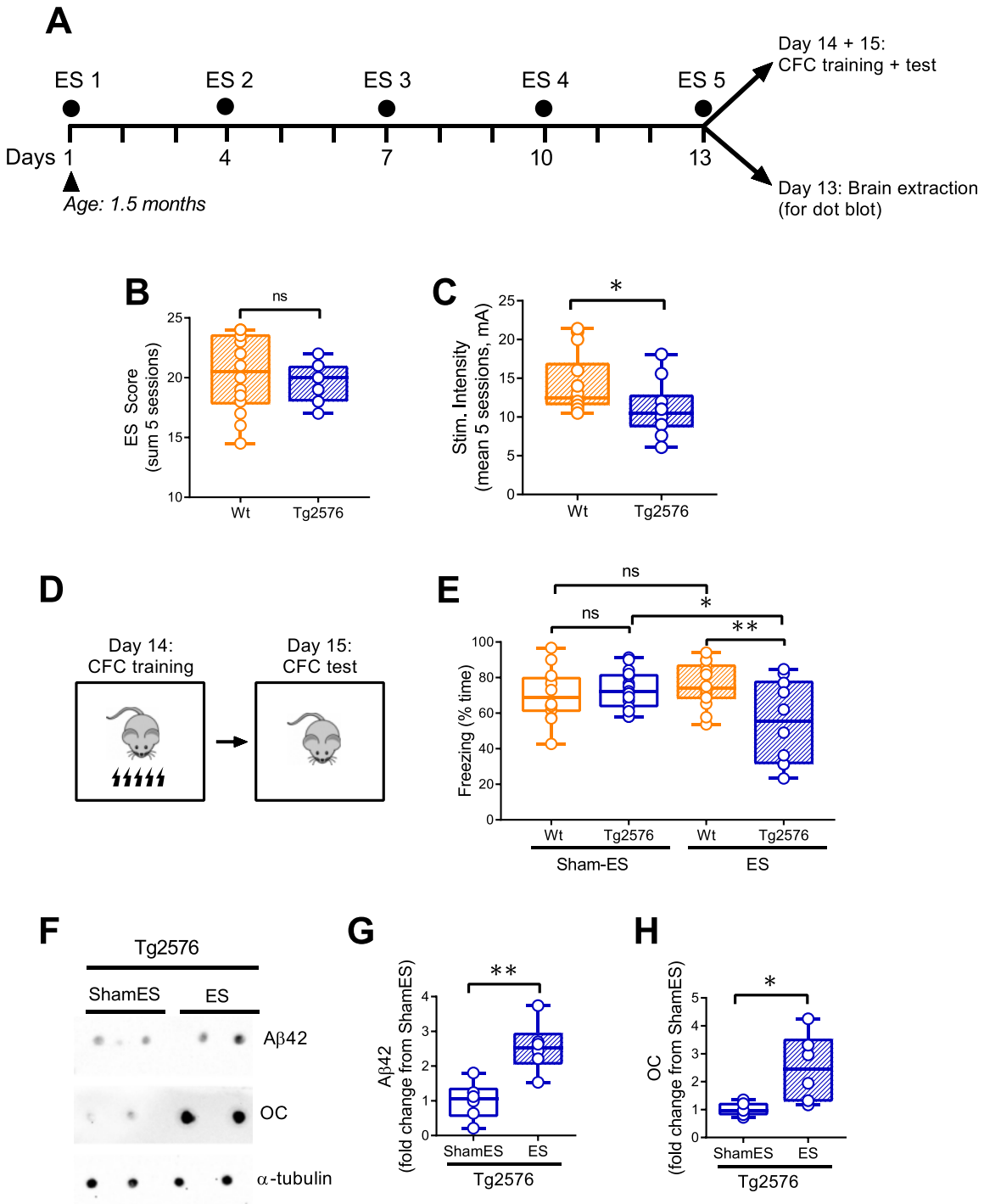

Fig. 1. Repeated seizures selectively impair memory performance in young Tg2576 male mice and increase fibrillar oligomeric Aβ load. A. Timeline of seizure induction and contextual fear conditioning (CFC) or brain extraction for dot blot analysis. Electroshock (ES)- induced seizures were obtained every 3 days, starting at 1.5 months of age, and lasted 13 days. Sham-ES mice were put in the ES cage, but no current was delivered through the earclips. B. Summary plot of the ES score, obtained by summing points from the Racine scale over the 5 sessions (see methods for details, Wt: $n = 14$, Tg2576: $n = 10$). C. Summary plot of the ES stimulation intensity (mean over 5 sessions) needed to obtain the scores reported in B. D. Schematic of CFC task. E. Summary plot of time spent freezing during the CFC test after equivalent seizure score in Wt and Tg2576 mice, in the sham condition or after ES (ShamES-Wt: $n = 14$, ShamES-Tg2576: $n = 15$, ES animals are the same as in panels B and C). F. Representative native dot blots from Tg2576 ShamES and ES animals. α-Tubulin was used as normalizing loading control. G. Quantification of $A\beta_{42}$ immunoreactivity obtained from native dot blot analysis with the anti-$A\beta_{42}$ antibody (clone 295F2). TBS hippocampal extracts from Tg2576 ES ($n = 6$, ES score = 21 ± 2) or ShamES ($n = 6$) littermate mice were obtained on day 13 of the protocol (Suppl. Fig. 1D). H. Quantification of Aβ immunoreactivity obtained from native dot blot analysis with the conformational OC antibody recognizing fibrillar oligomers. Same animals and procedure as in panel G. Data on graphs are represented as box plots with the median, boxes extending from the 25th to 75th percentiles, and whiskers extending from the smallest to the highest value.

minimum sample size of $n = 3$ (Fig. 1G and 5F) or 4 (Fig. 1H and 5G). For all other variables, d values were either moderate or large. Dot and western blot data were analyzed with the t-test/Mann-Whitney or with the one-way ANOVA and Fisher LSD post-hoc tests, depending on the number of groups compared. Errors associated with the percentage changes in firing were calculated with the propagation of error formula. A 95% confidence interval was used to assess statistical significance, represented on graphs as follows: n.s.: not significant; *: $p < 0.05$; **: $p < 0.01$; ***: $p < 0.001$.

3. Results

3.1. Tg2576 mice at pre-symptomatic stages are more susceptible to non-pharmacologically induced seizures

In order to be able to compare the effect of induced seizures on Tg2576 and Wt mice, we first confirmed that these animals did not exhibit spontaneous seizures at the age used for our experiments (i.e. 1.5–2 months). To this end, we video-recorded Tg2576 ($n = 11$) and Wt ($n = 8$) mice continuously for 2 weeks (timeline in Suppl. Fig. 1A) and scored behavior based on the Racine scale (Racine, 1972). No seizures were detected in either Wt or Tg2576 mice. This result is in line with previous studies (Bezzina et al., 2015; Kam et al., 2016) where seizures were observed in 7 month-old Tg2576 mice but not at 1.5–2 months of age when epileptiform activity was represented only by interictal events.

Thus, we devised a protocol to induce multiple, controlled seizures over several days. In this protocol, we made sure the following requirements were met. The first condition was to mimic the occurrence of several seizures. The second was that the Wt and the transgenic groups had to undergo an equivalent amount of seizures. These two requirements were obtained by exploiting the ES model, which consists in delivering electric stimuli through ear-clip electrodes. This method is commonly used with a one-trial test to assess the efficacy of anticonvulsant drugs (Castel-Branco et al., 2009), but it has also been used to investigate the effect of repeated seizures in rats (Cardoso et al., 2009; Jansson et al., 2009). We adapted it to induce multiple seizures in mice and observed that: a) it was reliable in inducing seizures; b) by grading the strength of current injection, it allowed reasonable control over the severity of seizures; c) it could be repeated over several days, without inducing convulsant *status epilepticus* (see methods for details). All mice undergoing this protocol received 5 ES sessions over 2 weeks, starting at 1.5 months of age (Suppl. Fig. 1B, C, D, G).

In a first experiment, we assessed seizure susceptibility of Tg2576 mice to the ES protocol, in comparison to Wt littermates (timeline in Suppl. Fig. 1B). Mice of the two genotypes received 5 ES starting at 1.5 months with, on average, the same intensity of stimulation (Wt: 23.8 ± 0.8 mA, $n = 27$, Tg2576: 21.4 ± 0.9 mA, $n = 36$, Suppl. Fig. 2A). Survival rate, calculated cumulatively in the 5 ES sessions, was lower in Tg2576 mice (21/36, 58.3%) when compared to Wt mice (23/27, 85.2%; Fisher's exact test: $p = 0.04$, Suppl. Fig. 2B).

In the following experiments, we aimed at investigating whether epilepsy plays a role in determining cognitive decline at otherwise pre-symptomatic stages of the disease. Thus, from here on, ES stimulation intensity was decreased in order to maximize survival rate (Fig. 1A and Suppl. Fig. 1C). Furthermore, at each session of the ES protocol, the intensity of stimulation was adjusted to induce the same total epileptic score in the two genotypes (Wt: 20.3 ± 0.9, $n = 14$; Tg2576: 19.6 ± 0.5, $n = 10$; unpaired *t*-test, $t_{22} = 0.65$, $p = 0.52$; Fig. 1B). This was done to ensure that the two groups had similar epileptic-like activity over the two weeks of ES induction. Given this experimental setting, the current each animal received in the 5 sessions was used as an indicator of susceptibility to seizures. The average current intensity at the end of the ES protocol was significantly lower for Tg2576 mice (11.1 ± 1.2 mA, $n = 10$) than for Wt littermates (14.3 ± 1.0 mA, $n = 14$, Mann-Whitney test, $U = 30$, $p = 0.017$; Fig. 1C). Overall, our data indicate that pre-symptomatic Tg2576 mice are more susceptible to epileptic seizures than Wt mice and are more vulnerable to seizure-induced death.

3.2. Seizures lead to memory impairment selectively in pre-symptomatic Tg2576 mice

The presence of epilepsy in patients with Alzheimer's disease correlates with an earlier onset and faster progression of cognitive decline (Irizarry et al., 2012; Vossel et al., 2016, 2013). To distinguish whether this is a nonspecific effect of seizures on memory impairment or is distinctively related to AD, we evaluated hippocampal dependent contextual memory after obtaining an equivalent seizure score in the Wt and the Tg2576 groups. This criterion was essential to test whether the same amount of epileptic seizures affects cognitive abilities differently in Wt and Tg2576 mice.

Contextual memory in Tg2576 mice is impaired at 3, but not 2, months (D'Amelio et al., 2011). Therefore, to assess whether seizures affect cognitive abilities of pre-symptomatic mice, Tg2576 and age-matched wild-types underwent the whole ES + CFC protocol between 1.5 and 2 months of age (see Fig. 1A and Suppl. Fig. 1C for a timeline). At the end of the seizure-induction protocol, the impact of repeated seizures on hippocampal dependent memory of Wt and Tg2576 mice was assessed with a CFC task (Fig. 1D). ShamES-Wt and ShamES-Tg2576 littermates also underwent CFC and were used as controls for stress associated with the ES manipulation. Freezing responses in the four groups, compared with a two-way ANOVA having genotype and treatment (ES/ShamES) as independent variables, were significantly different (genotype x treatment: $F_{1,35} = 5.82$, $p = 0.021$, Fig. 1E). Post-hoc analysis revealed that percentage of time spent freezing was not different between ShamES-Wt ($70.1 \pm 3.9\%$, $n = 14$) and ShamES-Tg2576 mice ($73.3 \pm 2.8\%$, $n = 15$; $p = 0.99$), confirming that 2 months old Tg2576 animals are at a pre-symptomatic stage of the disease. Importantly, freezing was also not significantly different between ShamES-Wt and ES-Wt mice ($p = 0.95$), indicating that ES-induced seizure activity *per se* had no effect on memory performance. We then evaluated whether recurrent seizures affected memory in the transgenic group. Indeed, time spent freezing in ES-Tg2576 mice ($54.9 \pm 7.4\%$, $n = 10$) was lower with respect to the ShamES-Tg2576 group ($p = 0.028$) and with respect to the ES-Wt group ($75.7\% \pm 3.3$, $n = 14$; $p = 0.010$), indicating that seizures have a different impact on memory in age-matched Wt and Tg2576 animals. More specifically, seizures mild enough to leave contextual memory unchanged in Wt mice cause cognitive impairment in pre-symptomatic AD mice. These results suggest that seizures accelerate cognitive decline in AD-susceptible mice, bringing the onset of detectable deficits to an earlier, otherwise asymptomatic, stage.

3.3. Aβ increases after ES-induced seizures in pre-symptomatic Tg2576 mice

Neuronal activity modulates the formation and secretion of Aβ peptides in neurons that overexpress APP (Kamenetz et al., 2003). Moreover, synaptic activity induced by focal seizures increases Aβ levels in the brain interstitial fluid *in vivo* (Cirrito et al., 2005). Thus, we investigated whether ES induced a modulation of Aβ oligomeric species in young Tg2576 mice (timeline in Suppl. Fig. 1D). For this purpose, we collected hippocampal samples of ES-Tg2576 and ShamES-Tg2576 mice and extracted proteins from the TBS soluble fraction (Meli et al., 2014; Pignataro et al., 2019).

Modulation of Aβ was investigated with a native dot blot analysis, performed with two different antibodies: a C-terminal-specific anti-$A\beta_{42}$

antibody (clone 295F2), which selectively detects $A\beta_{42}$ but no other Aβ/APP-truncated forms, and the OC antibody, which detects fibrillar oligomers (Kayed et al., 2007). With this assay, we found significant differences in $A\beta_{42}$ levels already in 2 months old naïve animals, when comparing hippocampi from Wt and Tg2576 animals ($t_4 = 4.6$, $p = 0.01$; Suppl. Fig. 3A,B). On the contrary, the more fibrillary species detected by OC were not different between the two genotypes at this age ($t_4 = 1.6$, $p = 0.19$; Suppl. Fig. 3A,C).

Tg2576 animals undergoing the ES protocol exhibited a 2.5-fold increase in $A\beta_{42}$ with respect to ShamES-Tg2576 mice (ShamES-Tg2576: 1.00 ± 0.22, $n = 6$ *vs* ES-Tg2576: 2.54 ± 0.29, $n = 6$; *t*-test, $t_{10} = 4.18$, $p = 0.0019$; Fig. 1F, G). Similarly, OC positive signals increased in ES-Tg2576 mice as compared to control ShamES-Tg2576 by a similar amount (ShamES-Tg2576: 1.00 ± 0.09, $n = 6$ *vs* ES-Tg2576: 2.49 ± 0.49, $n = 6$; t-test, $t_{10} = 2.95$, $p = 0.015$; Fig. 1F, H). Interestingly, the increase in $A\beta_{42}$ induced at 2-months by seizures was comparable to the one spontaneously shown by 3-months old naïve mice (one-way ANOVA: $F_{3,12} = 3.96$ $p = 0.035$; post-hoc: ShamES-Tg2576 *vs* ES-Tg2576 p = 0.015; ES-Tg2576 *vs* 3 month-old Tg2576 $p = 0.92$; Suppl. Fig. 3D, E), while levels of OC positive species were significantly higher in 2-months old ES-Tg2576 mice with respect to 3-months old naïve mice (one-way ANOVA: $F_{3,12} = 9.39$ $p = 0.002$; post-hoc, ShamES-Tg2576 *vs* ES-Tg2576: $p = 0.013$; ES-Tg2576 *vs* 3 month-old Tg2576: $p = 0.003$; Suppl. Fig. 3D,F), indicating that seizures induce a particularly accelerated production of fibrillary, more toxic, species. On the other hand, no differences were detected in $A\beta_{42}$ and OC signals between ShamES- and ES-Wt mice ($A\beta_{42}$: Mann-Whitney, U = 4, $p > 0.99$; OC: Mann-Whitney, U = 4, $p > 0.99$, Suppl. Fig. 3G–I). Collectively, this set of experiments indicates that $A\beta_{42}$ and OC-positive fibrillary species increased in the extracellular fraction of the hippocampus upon exposure to ES only in Tg2576 and not in Wt animals.

Along with Aβ, also APP accumulation is associated with alterations of neuronal activity and seizures in both humans and rodents (Born et al., 2014; Westmark, 2013). Thus, we evaluated whether APP levels are altered by the ES treatment, by performing a western blot analysis on the TBS soluble fraction with 22C11, an antibody that detects both the wild-type and the mutated APP isoforms (Suppl. Fig. 4). Seizures increased APP levels in 2 months old Tg2576 mice but not in Wt littermates (one-way ANOVA, $F_{4,14} = 8.46$, $p = 0.001$; post-hoc: ShamES-Wt *vs* ES-Wt: $p = 0.72$; ShamES-Tg2576 *vs* ES-Tg2576: $p = 0.02$). APP levels in 2 months old ES-Tg2576 were similar to levels in 3 months old, naïve mice (post-hoc: $p = 0.68$).

3.4. Intrinsic cellular excitability of CA1 neurons in pre-symptomatic Tg2576 mice is enhanced

The higher susceptibility of Tg2576 mice to seizures in the pre-symptomatic stage and the memory decline induced selectively in this group by the ES protocol indicate that Tg2576 brain cells undergo modifications prior to the appearance of memory deficits. We therefore investigated possible alterations in neuronal signaling in the hippocampus, a region underlying formation of contextual memory (Maren et al., 2013) and involved in the response to ES induction (Chawla et al., 2013). Experiments were performed without induction of any seizures, with the aim of revealing neuronal alterations exclusively linked to disease progression and not to the seizures themselves (timeline in Suppl. Fig. 1E). The rationale is that alterations found at this non-symptomatic stage could possibly underlie higher seizure susceptibility and, later in the disease progression, become so widespread that memory deficits become manifest.

We performed whole cell patch-clamp recordings from CA1 pyramidal neurons in acute slices obtained from Tg2576 mice and from their Wt littermates at pre-symptomatic stages, i.e. 1 month of age. Firing was analyzed in response to depolarizing current injections (Fig. 2A). Cells from pre-symptomatic Tg2576 mice exhibited significantly higher number of spikes with respect to Wt cells over the range of stimulation intensities tested (50–700 pA; two-way ANOVA, genotype effect: $F_{1,443} = 52.85$, $p < 0.0001$; stimulus intensity effect: $F_{13,443} = 30.78$, $p < 0.0001$; genotype x stimulus intensity: $F_{13,443} = 0.83$; $p = 0.63$, Wt: $n = 21$, Tg2576: $n = 15$). These data indicate that CA1 pyramidal cells are characterized by significantly higher intrinsic excitability at the pre-symptomatic stage.

In order to investigate the mechanisms giving rise to hyper-responsive Tg2576 CA1 pyramidal neurons, we analyzed basic passive and active electrophysiological properties in Wt and Tg2576 cells (see Table 1 for results). While resting membrane potential (RMP) and *rheobase* current were not significantly different between the two genotypes, R_{in} was significantly lower in cells from transgenic mice. Moreover, Tg2576 neurons exhibited significantly lower action potential duration, measured at half-width, and increased decay slope. Coherently, the fAHP latency was significantly shorter in Tg2576 cells compared to Wt.

Further analysis revealed that the mAHP exhibited significantly lower amplitude in the Tg2576 group (5.83 ± 0.42 mV, $n = 15$) when compared to Wt (8.36 ± 0.63 mV, $n = 15$; unpaired *t*-test, $t_{28} = 3.37$, $p = 0.02$; Fig. 2B), during repetitive firing at low spike frequencies. Indeed, mAHP has been shown to regulate firing frequency in CA1 pyramidal neurons, through Kv7/KCNQ/I_M and HCN/I_h currents (Gu et al., 2005). While both classes of channels are involved in memory and in epilepsy (He et al., 2014; Peters et al., 2005), a recent proteomics meta-analysis on AD patients revealed that HCN1 downregulation is one the few consistent and robust alterations observed in the human AD proteome (Haytural et al., 2021). Thus, we investigated whether an impairment in HCN channels might already be present at these early non-symptomatic stages in our AD mouse model. To address this question, we first analyzed the voltage sag, i.e. a slow relaxation of the membrane potential in response to long hyperpolarizing current steps (Fig. 2C). The sag is due to the activation of the hyperpolarization activated cation current I_h and its magnitude is an index of the level of HCN channel activity. In response to hyperpolarizing current steps, the sag in Tg2576 cells was significantly smaller than in Wt cells (two-way ANOVA, $F_{1,26} = 5.44$, $p = 0.028$; Fig. 2D). Of note, the post-inhibitory rebound peak, which has also been shown to depend on I_h activation (Ascoli et al., 2010), was significantly smaller in Tg2576 neurons (3.11 ± 0.33 mV, $n = 14$) than in Wt cells (4.36 ± 0.52 mV, $n = 14$; unpaired *t*-test, $t_{26} = 2.03$, $p = 0.053$; Fig. 2E). This result indicates that HCN channels underlying the I_h current are less active in transgenic cells at 1 month of age.

Of the four HCN subunits (HCN1–4) that have been identified so far, HCN1 is abundantly expressed, among other areas, in the hippocampus (Moosmang et al., 1999). We therefore investigated whether the decrease in current might be due to lower expression of these channels, by performing western blot analysis of the HCN1 subunit, specifically from the CA1 area (timeline in Suppl. Fig. 1F). Indeed, expression of HCN1 was significantly reduced in 1 month old Tg2576 mice with respect to Wt littermates (Wt: 1.00 ± 0.11, $n = 12$, Tg2576: 0.62 ± 0.10, $n = 11$; unpaired *t*-test, $t_{21} = 2.54$, $p = 0.019$; Fig. 2F). Notably, lower protein amounts were not paralleled by changes in HCN1 mRNA levels (Wt: 1.00 ± 0.09, $n = 18$, Tg2576: 0.99 ± 0.10, $n = 13$; unpaired t-test, $t_{29} = 0.015$, $p = 0.98$; Fig. 2G). This suggests that the observed decrease in HCN1 protein occurs at the translational or post-translational level.

Together, these data demonstrate that Tg2576 CA1 pyramidal cells exhibit increased excitability in comparison to Wt cells, at a time when hippocampal-dependent memory is still intact in these mice. This increase correlates with a significant decrease of the mAHP, the I_h current and with lower levels of the underlying HCN channels.

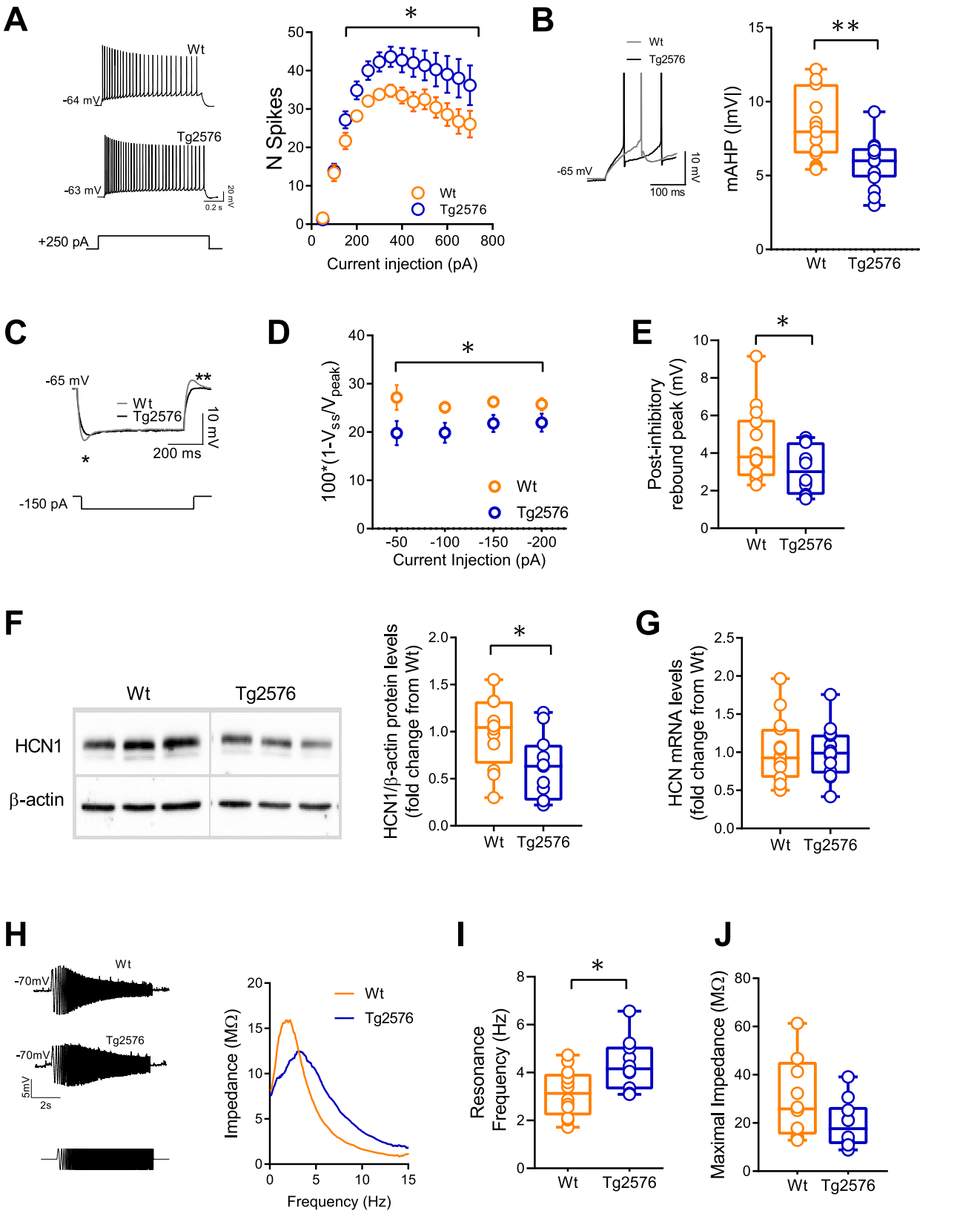

(caption on next page)

Fig. 2. Electrophysiological alterations in CA1 pyramidal neurons of pre-symptomatic male and female Tg2576 mice. A. Intrinsic excitability was significantly higher in Tg2576 than in Wt neurons of 1–2 months old animals. Left: example traces in response to a positive current step (+250 pA). Right: summary plot of number of spikes *vs* positive current injections [Wt: $n = 21$ cells (from 11 animals), Tg2576: $n = 15$ (8)]. B. The medium afterhyperpolarization (mAHP) was significantly lower in Tg2576 *vs* Wt cells. Left: example traces in response to a low intensity positive current step (+100 pA). Right: summary plot of mAHP values [Wt: $n = 15$ (11), Tg2576: $n = 15$ (8)]. C. Example traces in response to a negative current step (−150 pA). * indicates sag; ** indicates post-inhibitory rebound peak. D. Summary plot of voltage sag values *vs* current intensity. V_{ss}: membrane voltage measured at steady-state, in response to a negative current step; V_{peak}: membrane voltage measured at the negative peak of the same response [Wt: $n = 15$ (11), Tg2576: $n = 15$ (8)]. E. Summary plot of post-inhibitory rebound peak in response to a negative current step (−150 pA). F. HCN1 protein levels were significantly lower in the CA1 region of Tg2576 *vs* Wt mice. Left: representative western blots of Wt and Tg2576 CA1 lysates. Right: Summary plot of HCN1 levels, normalized to β-actin (each dot represents a lysate from a different brain, Wt: $n = 12$, Tg2576: $n = 11$). These samples were also used to extract total RNA and perform qRT-PCR. G. Summary plot of HCN1 mRNA levels (normalized to GAPDH mRNA; Wt: $n = 18$, Tg2576: $n = 13$). H. Representative responses to a ZAP protocol. Left: membrane voltage of a Wt and Tg2576 pyramidal cell in response to a sinusoidal current with linearly increasing frequency (lower trace). Right: impedance amplitude profile of the same two cells as a function of the input frequency. Impedance was calculated as the ratio of the Fast Fourier transforms (FFT) of the voltage response and of the current injection. I. Summary plot of average resonance frequency [Wt: $n = 12$ (6), Tg2576: $n = 10$ (6)]. J. Summary plot of maximal impedance (maximum of the impedance profile, same cells as in I). Data on graphs are represented as box plots with the median, boxes extending from the 25th to 75th percentiles, and whiskers extending from the smallest to the highest value.

Table 1
Electrophysiological characteristics of *ex vivo* CA1 pyramidal neurons from 1.5 month old Tg2676 mice.

Electrophysiological properties	Wt	(n/N)	Tg2576	(n/N)	p
RMP (mV)	−62.1 ± 1.3	(31/15)	−63 ± 1.2	(28/15)	0.98
R_{in} (MΩ)	**142 ± 7**	**(36/18)**	**120 ± 7**	**(32/17)**	**0.026**
Rheobase current (pA)	67 ± 5	(36/18)	73 ± 5	(32/17)	0.41
Spike Amplitude (mV)	90.8 ± 1.9	(36/18)	91.3 ± 2.4	(30/17)	0.86
Spike Threshold (mV)	−44.9 ± 0.6	(36/18)	−45.9 ± 0.6	(30/17)	0.21
Half Width (ms)	**0.95 ± 0.04**	**(36/18)**	**0.84 ± 0.02**	**(30/17)**	**0.016**
Rise Slope (mV/ms)	285 ± 15	(36/18)	287 ± 13	(30/17)	0.98
Decay Slope (mV/ms)	**−82.1 ± 3.4**	**(36/18)**	**−91.5 ± 2.4**	**(30/16)**	**0.026**
fAHP Amplitude (mV)	−6.72 ± 0.46	(32/15)	−5.79 ± 0.54	(28/15)	0.19
fAHP latency (ms)	**2.34 ± 0.08**	**(32/15)**	**2.03 ± 0.05**	**(28/15)**	**0.002**
ADP (mV·ms)	7.9 ± 0.5	(21/10)	7.6 ± 0.6	(20/9)	0.732

For each parameter, mean ± SEM values and number of cells in parenthesis are given. All data were normally distributed; thus the *p* value was calculated with an unpaired *t*-test. RMP: Resting Membrane Potential; R_{in}: input resistance; fAHP: fast afterhyperpolarization; ADP: afterdepolarization; n: number of neurons; N = Number of animals. Bold indicates statistically significant differences.

3.5. Subthreshold electrical resonance is altered in CA1 neurons of pre-symptomatic Tg2576 mice

Resonance is the property by which a neuron, subjected to an oscillatory input, responds with greater intensity at certain preferred input frequencies with respect to others (Hutcheon and Yarom, 2000). CA1 pyramidal neurons exhibit resonance properties at frequencies in the theta range (2–7 Hz) (Hu et al., 2009, 2002), known to support hippocampal-dependent learning and memory (Buzsáki and Moser, 2013; Kragel et al., 2020). Since subthreshold resonance in CA1 pyramidal neurons strongly depends on HCN channels (Hu et al., 2002; Nolan et al., 2004), we investigated whether these exhibit differences in Tg2576 and Wt cells. To this end, we applied a "ZAP" protocol during whole-cell current-clamp recordings (Hu et al., 2002), which consisted in a sinusoidal current with constant amplitude and linearly increasing frequency (0.5–15 Hz, lasting 30 s; ZAP current) injected into cells clamped at −70 mV. Resonance was detected as a distinct and reproducible peak in the voltage response (Fig. 2H) at a point corresponding to a frequency of 3.16 ± 0.28 Hz ($n = 12$) in Wt and 4.33 ± 0.34 Hz ($n = 10$) in Tg2576 (unpaired *t*-test, $t_{20} = 2.67$, $p = 0.015$; Fig. 2I). The impedance profile (the relationship between the voltage response and the input current as a function of the frequency) calculated by dividing the FFT of the voltage response by the FFT of the input ZAP current showed a peak value of 29.7 ± 4.6 MΩ in Wt and 19.4 ± 3.1 MΩ in Tg2576 mice (unpaired *t*-test, $t_{20} = 1.76$, $p = 0.09$; Fig. 2H, J). These results suggest that the decrease observed in the I_h could account for alterations in the resonance properties of CA1 cells. This could in turn impair the ability of the hippocampal circuit to engage in brain rhythms such as theta oscillations, relevant for memory (Buzsáki, 2002; Buzsáki and Moser, 2013).

3.6. LTG restores intrinsic excitability of Tg2576 CA1 pyramidal neurons to wild type levels

LTG is an anti-epileptic drug that has been shown to upregulate HCN channel activity in CA1 pyramidal cells (Poolos et al., 2002). Thus, we investigated whether the increased excitability observed in these neurons could be restored to Wt levels by bath-applying LTG to Tg2576 slices coming from 1.5 months old mice, i.e. the age at which animals received the ES protocol. We first ensured that LTG (100 μM) was effective in acting on HCN channels by measuring the I_h–dependent sag before and after application of the drug. Indeed, LTG led to a significant increase of sag amplitudes in Tg2576 cells (from 25.6 ± 1.5 to 27.5 ± 1.6, $n = 11$; paired t-test, $t_{10} = 2.60$, $p = 0.02$; Fig. 3A) and of the post-inhibitory rebound peak (from 4.35 ± 0.51 mV to 6.44 ± 0.75 mV, $n = 11$; paired t-test, $t_{10} = 5.79$, $p = 0.0002$). Sag levels in the presence of the drug were comparable to the Wt values reported in the previous section (Fig. 3B; one-way ANOVA: $F_{3,50} = 2.56$, $p = 0.035$; post-hoc: Wt *vs* Tg2576 + LTG: $t_{50} = 0.59$, $p = 0.80$, Tg2576 *vs* Tg2576 + LTG: $t_{50} = 2.39$, $p = 0.04$). Secondly, we investigated the effect of LTG on the mAHP and on the number of spikes evoked by depolarizing current steps. We found that LTG increased the mAHP from −5.76 ± 1.85 mV to −7.67 ± 2.1 mV ($n = 11$, $p = 0.04$, Wilcoxon paired test, Fig. 3C). As for the sag, the mAHP of Tg2576 cells recorded with LTG was not significantly different than the value for the Wt control group (Fig. 3D; one-way ANOVA: $F_{2,56} = 11.43$, $p < 0.0001$; post-hoc: Wt *vs* Tg2576 + LTG: $p = 0.72$, Tg2576 *vs* Tg2576 + LTG: 0.01). Finally, LTG significantly reduced the number of action potentials in response to 1 s current injections at 50–700 pA intensities (two-way ANOVA: $F_{13,\ 221} = 1.784$, p = 0.04; Fig. 3E). In this interval, the average number of spikes had a percent reduction due to LTG of 33 ± 3%, a value comparable to the percent increase in firing calculated between Wt and Tg2576 cells (29.4 ± 0.4%). Therefore, LTG was able to decrease CA1 Tg2576 pyramidal neuron firing responses by the amount needed to restore firing to Wt levels. Finally, resonance frequency was significantly decreased from 3.81 ± 0.07 Hz to 3.42 ± 0.13 Hz in 12 cells (paired t-test, $t_{11} = 4.50$, $p = 0.0009$; Fig. 3F–G). When compared to the Wt group, resonance frequency was restored to control levels (one-way ANOVA: $F_{2,53} = 7.41$, $p = 0.002$; post-hoc: Wt *vs* Tg2576 + LTG: $t_{53} = 0.64$, $p = 0.78$; Fig. 3H). Overall, these results indicate that LTG rescues alterations in Tg2576 CA1 pyramidal neuron signaling in acute slices.

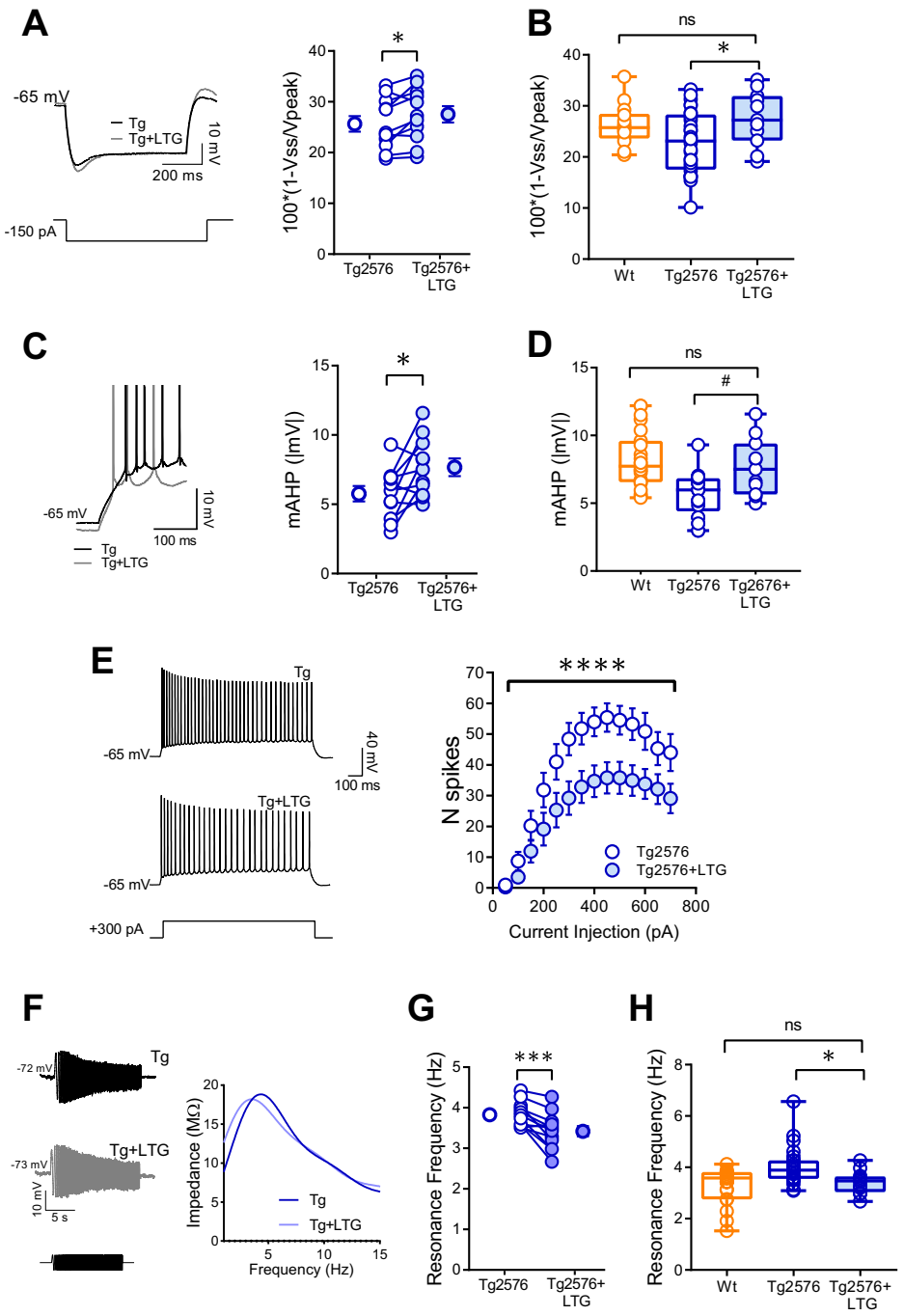

Fig. 3. Lamotrigine (LTG) rescues electrophysiological alterations of male and female Tg2576 CA1 pyramidal neurons *ex vivo*. A. The I_h sag of Tg2576 cells was significantly increased by bath application of LTG. Left: representative traces before and after bath application of LTG in response to a negative current step (−150 pA). Right: Mean sag ± SEM and values for cells with paired control and LTG conditions are shown [$n = 11$ (from 7 animals)]. B. Bath application of LTG restores sag values of Tg2576 cells to Wt levels. Summary plot for cells from independent, unpaired experiments [Wt: $n = 15$ (11), Tg2576: $n = 28$ (17), Tg2576 + LTG: $n = 11$ (7)]. C. Tg2576 mAHP was increased by LTG. Left: representative traces of the response of a Tg2576 cell to a positive current step (+100 pA) before and after bath application of LTG (spikes truncated). Right: Mean mAHP ± SEM and values for cells with paired control and LTG conditions are shown [$n = 11$ (7)]. D. LTG restores mAHP of Tg2576 neurons to levels similar to Wt. Summary plot for cells from independent, unpaired experiments [Wt: $n = 23$ (18), Tg2576: $n = 25$ (15), Tg2576 + LTG: $n = 11$ (7); #: $p = 0.07$]. E. LTG significantly decreased the number of action potentials in response to positive current steps. Left: representative trace in response to a positive current step before and after LTG application. Right: summary plot of the number of spikes *vs* current intensity for cells before and after bath application of LTG [$n = 11$ (7)]. F. Response to a ZAP protocol in the absence and presence of LTG. Left: representative traces of a Tg2576 neuron injected with a sinusoidal current with linearly increasing frequency before and after LTG application. Right: impedance profile for the cell shown on the left. G. Bath application of LTG significantly shifted the resonance frequency of Tg2576 neurons. Mean resonance frequency ± SEM and values for cells with paired control and LTG conditions are shown [$n = 12$ (7)]. H. Bath application of LTG restored resonance frequency of Tg2576 cells to Wt levels. Summary plot for cells from independent, unpaired experiments [Wt: $n = 19$ (14), Tg2576: $n = 25$ (14), Tg2576 + LTG: $n = 12$ (7)]. Data on graphs are represented as box plots with the median, boxes extending from the 25th to 75th percentiles, and whiskers extending from the smallest to the highest value.

To gain further insight on the mechanisms through which LTG restores the observed parameters, in a separate set of experiments LTG was administered to Wt neurons to observe its direct effect on these cells. Contrary to Tg2576 neurons, the average sag value in Wt cells was not altered by LTG (paired t-test, $t_{25} = 1.23$, $p = 0.23$, Fig. 4A). When analyzing the percentage of cells in which LTG did increase the sag value (Fig. 4B), this was indeed much lower in Wt cells (38%) than in Tg2576 cells (65%; Fisher exact test: $p = 0.0002$). Likewise, LTG did not induce a significant change in the mAHP (paired t-test, $t_{10} = 1.34$, $p = 0.21$, Fig. 4C) or in the resonance frequency of Wt cells (paired t-test, $t_{10} = 0.89$, $p = 0.40$, Fig. 4D). On the contrary, LTG decreased the number of spikes in all cells (100%) and this effect was significant (two-way ANOVA, treatment: $F_{1,672} = 480.9$, stimulation intensity: $F_{15,672} = 31.05$, $p < 0.0001$, stimulation intensity x treatment: $F_{15,672} = 2.189$, $p = 0.0057$; Fig. 4E). This last result suggests that: (i) LTG was indeed exerting an action on all cells (i.e. the lack of an effect on the sag or on other parameters was not due to a general lack of action of the drug); (ii) the mechanism by which the number of spikes decreased was not only through an increase in the I_h, in line with data from others (Kazmierska-Grebowska et al., 2021). Indeed, LTG has also been shown to inhibit Na^+ currents through a slow binding to the fast-inactivated state of Na^+ (Kuo and Lu, 1997). Because this mechanism is use-dependent, we analyzed the instantaneous frequency of the action potentials as a function of spike number in response to a 300 pA depolarizing step. The analysis shows that the instantaneous frequency of the first spike in the absence or presence of LTG was similar, while the gap between the two values increased at each spike, becoming significant after the 8th spike (Fig. 4F). This result is consistent with the use-dependent action of LTG on Na^+ channels.

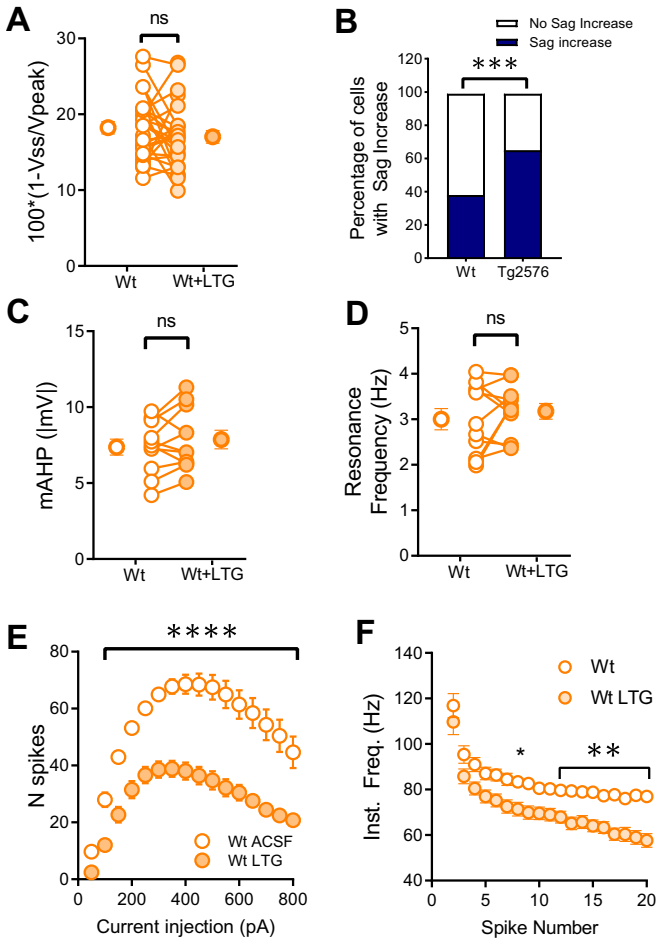

Fig. 4. Lamotrigine (LTG) affects electrophysiological properties of *ex vivo* Wt CA1 pyramidal neurons differently than Tg2576 mice.
Experiments were performed on neurons coming from both male and female mice. A. I_h-dependent sag in response to a − 150 pA current injection was not significantly different for Wt cells in ACSF and in the presence of LTG [100 μM; $n = 26$ (16)]. Paired values refer to the same cell. Mean sag ± SEM for the two conditions are also shown. B. Percentage of Wt and Tg2576 CA1 neurons in which LTG induced an increase in the sag. C—D. The medium AHP (mAHP) and the resonance frequency were not significantly different for Wt cells in ACSF and in the presence of LTG. Paired values refer to the same cell. Mean sag ± SEM for the two conditions are also shown [$n = 11$ (8)]. E. Summary plot (mean ± SEM) of the number of action potentials fired in response to a 1 s depolarizing step in Wt cells recorded in ACSF or ACSF+LTG [$n = 22$ (12)]. F. Mean instantaneous frequency calculated for each action potential fired in response to a 300 pA depolarizing step, in ACSF and ACSF+LTG. *$p < 0.05$, **$p < 0.01$, ***$p < 0.001$, ****$p < 0.0001$.

3.7. LTG prevents seizure-induced CFC memory deficits in pre-symptomatic Tg2576 mice

The observation that LTG rescues hyper-excitability and resonance alterations of Tg2576 CA1 neurons *ex vivo* prompted us to investigate whether *in vivo* treatment with LTG could act as a disease-modifying drug in Alzheimer's disease mice undergoing epileptic seizures. More specifically, we asked whether LTG administration could prevent the memory deficits induced by seizures in 2 months old Tg2576 mice.

To test this hypothesis, we injected ES-Tg2576 mice with LTG or VEH once a day starting eight days before the first ES session and for the whole duration of the protocol, corresponding to 5 ES and 2 CFC sessions (total treatment duration: 23 days, see Fig. 5A and Suppl. Fig. 1G for a timeline). As a control for the effect of LTG, littermate Wt animals undergoing the ES protocol were also injected with VEH (VEH-ES-Wt) or LTG (LTG-ES-Wt).

At every ES session, stimulus intensity for each animal was adjusted to obtain the same total seizure score between the four groups (one-way ANOVA: $F_{3,35} = 0.76$, $p = 0.52$; Fig. 5B). In this experimental setting, differences in seizure susceptibility were assessed from the stimulus intensity necessary to obtain the same final seizure score in the four groups. Indeed, LTG increased the threshold for seizure generation in both the Wt and the Tg2576 groups (one-way ANOVA: $F_{3,35} = 0.2029$, $p < 0.0004$, VEH-ES-Wt *vs.* LTG-ES-Wt: $p = 0.012$, VEH-ES-Tg2576 vs. LTG-ES-Tg2576: $p = 0.002$; Fig. 5C), confirming the anti-convulsive action of this drug. Next, we tested the potential of LTG in preventing seizure-induced cognitive impairment. To this end, animals were subjected to the CFC task after LTG administration and the ES protocol. Significant differences in freezing levels were found among the four groups (two-way ANOVA, genotype: $F_{1, 35} = 8.14$, $p = 0.0049$, genotype x treatment: $F_{1, 35} = 9.03$, $p = 0.007$; Fig. 5D). With a post-hoc analysis, we first confirmed that seizures induced memory deficits in 2 months old VEH treated Tg2576 mice (VEH-ES-Wt: 81 ± 3%, $n = 13$ *vs* VEH-ES-Tg: 52 ± 5%, $n = 9$; $t_{35} = 4.51$, $p < 0.0001$). Next, we compared memory performance in LTG- and VEH-treated Tg2576 mice. Indeed, freezing levels in the LTG-ES-Tg group (69 ± 5%, $n = 11$) were significantly higher with respect to the control VEH-treated Tg animals ($t_{35} = 2.36$, $p = 0.02$), and not different from the LTG-ES-Wt group (69 ± 8%, $n = 6$; $t_{35} = 0.10$, $p = 0.92$), indicating that LTG prevented seizure-induced memory deficits in Tg2576 mice. Because LTG- and VEH- treated Tg2576 animals had similar seizure scores, our results also demonstrate that LTG prevented seizure-induced memory deficits not by a simple decrease of seizure occurrence.

To test whether LTG treatment also modulated extracellular $A\beta_{42}$ oligomers and OC-positive fibrillary species, we quantified hippocampal protein extracts with both the $A\beta_{42}$ and OC antibodies (Fig. 5E–G, timeline in Suppl. Fig. 1G). Remarkably, LTG treatment prevented the rise of extracellular Aβ induced by seizures, detected by both the $A\beta_{42}$ and the OC antibodies (one-way ANOVA, $A\beta_{42}$: $F_{2,15} = 9.30$, $p = 0.0024$; OC: $F_{2,15} = 14.94$, $p = 0.0003$; post-hoc: LTG- *vs* VEH-treated group, $A\beta_{42}$: 1.38 ± 0.06 *vs* 2.52 ± 0.37, $t_{15} = 3.15$, $p = 0.013$; OC: 0.93 ± 0.13 *vs* 2.55 ± 0.38; $p = 0.0004$, $n = 6$, normalized to ShamES; LTG-treated *vs* ShamES, $A\beta_{42}$: 1.00 ± 0.25, $t_{15} = 0.97$, $p = 0.57$; OC: 1.00 ± 0.08; $p = 0.98$, $n = 6$).

Collectively, these experiments demonstrate that LTG not only increases seizure threshold but also prevents the memory deficits and accumulation of Aβ fibrillar oligomers induced by seizures in the early phases of the disease in human APP overexpressing mice.

4. Discussion

We investigated whether cellular alterations involved in early hippocampal hyperactivity leading to epilepsy could also be responsible for memory impairment in AD. We used the Tg2576 mouse model at pre-symptomatic stages, i.e. 1–2 months of age. Although this corresponds to a young age in humans, functional brain alterations in patients have been shown to begin decades before the clinical onset of AD (reviewed in Palop and Mucke, 2016) and as soon as 20 years of age (Filippini et al., 2009).

We first confirmed that pre-symptomatic Tg2576 AD mice are more susceptible to epileptic seizures than age-matched Wt animals, in line with previous reports (Bezzina et al., 2015) and with a high comorbidity of epilepsy in AD patients (Vossel et al., 2017). Moreover, repeated seizures triggered the onset of memory decline in Tg2576 but not in Wt mice at an early, otherwise non-symptomatic, age providing evidence that epileptic seizures play an active role in triggering disease manifestation. This result is in line with the clinical observation that AD patients with seizures have an onset of symptoms that is on average 5.5 years earlier than non-epileptic patients (Vossel et al., 2013).

We induced recurrent seizures with the ES protocol, which offers several advantages over chemoconvulsants. First, it provides a general

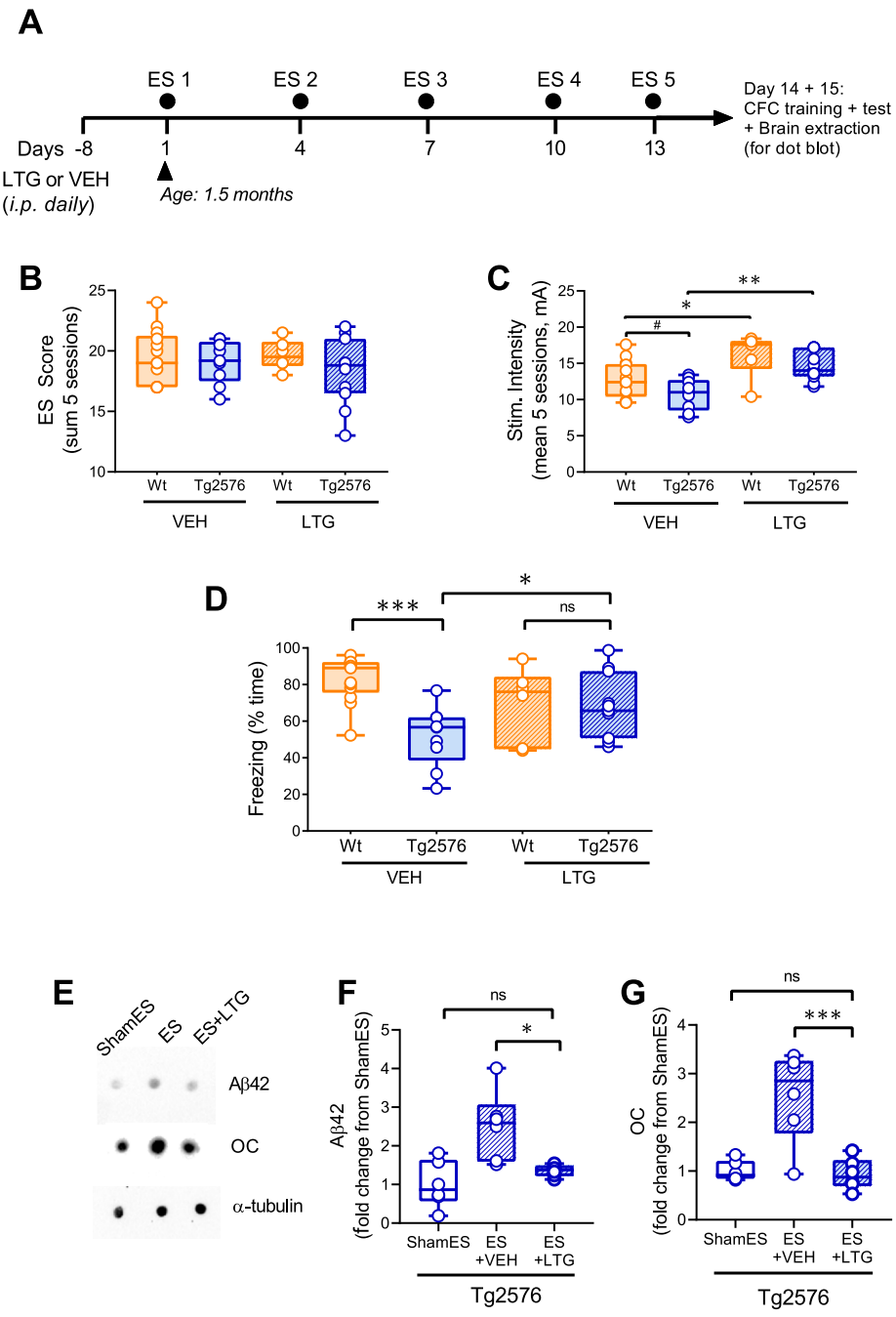

Fig. 5. Lamotrigine (LTG) prevents ES-induced memory impairment and Aβ release in male Tg2576 mice. A. Timeline of the experimental protocol involving intraperitoneal (i.p.) injection of LTG or vehicle (VEH), ES induction and memory testing through CFC, in Wt and Tg2576 animals. All animals survived. B. Summary plot of the ES score, obtained by summing points from 5 ES sessions for Wt and Tg2576 mice treated with VEH or LTG (VEH-ES-Wt: $n = 13$, VEH-ES-Tg: $n = 9$, LTG-ES-Wt: $n = 6$, LTG-ES-Wt: $n = 11$). C. Summary plot of the ES stimulation intensity (mean over 5 sessions) needed to obtain the scores reported in B (#: $p = 0.06$). D. Summary plot of time spent freezing during the CFC test after equivalent seizure score in Wt and Tg2576 mice treated with VEH or LTG (same animals as in B and C). E. Representative native dot blots from Tg2576 ShamES, ES or LTG-treated ES mice. α-Tubulin was used as normalizing loading control. F. Quantification of $A\beta_{42}$ immunoreactivity obtained from native dot blot analysis with the anti-$A\beta_{42}$ antibody (ShamES-Tg: $n = 6$, ES-VEH: $n = 6$, or ES-LTG: $n = 6$). G. Quantification of OC immunoreactivity obtained from native dot blot analysis with the conformational antibody recognizing fibrillar oligomers. Same procedure as in F. Data on graphs are represented as box plots with the median, boxes extending from the 25th to 75th percentiles, and whiskers extending from the smallest to the highest value.

stimulus to the network rather than the activation of a specific channel/receptor, which could *per se* be altered in the pathology, allowing to gain knowledge on the susceptibility of the network without a bias due to the use of a specific pro-convulsive drug. Second, through a fine control of the intensity of stimulation, it is possible to adjust the amount of seizures each animal experiences. Finally, seizures could be induced over weeks, allowing to mimic recurrent seizures that might occur in the human pathology. The last two conditions were essential to obtain the same seizure score over several sessions in the different groups of animals tested (Wt vs Tg2576, VEH *vs* LTG) and thus to dissect the role of genotype or treatment in seizure-induced triggering of memory deficits.

We hypothesized that the cellular alterations determining the higher susceptibility of Tg2576 mice to seizures could be the same ones that later contribute to memory impairment. Although we cannot exclude deficits in the function of other channels known to regulate intrinsic excitability, e.g. Kv7/KCNQ/I_M channels (Alcantara-Gonzalez et al., 2021), our data support a role for altered HCN/I_h activity at early non-symptomatic stages of AD, as shown by lower I_h responses and decreased HCN1 protein levels in hippocampal CA1. Of note, these changes are not paralleled by modifications of HCN1 mRNA levels, indicating that APP/Aβ overexpression does not alter transcription or stability of HCN1 mRNA. Rather, it suggests that either HCN1 translational efficiency or protein turnover are affected in Tg2576 mice. Further analyses will be necessary to ascertain which molecular mechanism is responsible for HCN1 protein deficiency in AD and the underlying causes. The importance of this issue is warranted by a recent meta-analysis revealing that HCN1 downregulation is one of the most consistent and robust changes observed in the human AD proteome (Haytural et al., 2021).

The role of HCN alterations in determining epilepsy is well established, with HCN1 loss-of-function leading to increased excitability and

epilepsy in both humans and animals (Huang et al., 2009; Marini et al., 2018). HCN channels also play a role in memory, with a different modulatory action depending on the learning task and the circuitry involved (Chang et al., 2019). Specifically, forebrain deletion of HCN1 leads to increased spatial learning (Nolan et al., 2004). Yet, AD has been shown to progressively affect brain structures starting from mediotemporal areas including the hippocampus. Therefore, I_h decline in the early phases of AD, such as the one of this study, could be restricted to a much smaller area that affects memory differently. Moreover, chronic cerebral hypoperfusion, an AD-related model of dementia, induces spatial learning and memory deficits in rats, accompanied by a reduction of HCN1 channels in the CA1 region in the early phases after the insult (Luo et al., 2015). In this model, restoring HCN1/HCN2 surface expression rescued cognitive performance (Li et al., 2014). Moreover, HCN1 levels have been found to be consistently decreased in the temporal lobe of AD patients (Haytural et al., 2021; Saito et al., 2012).

We investigated the effect of LTG on electrophysiological properties *ex vivo*, on seizures susceptibility and on cognitive performance. This AED has been shown to have beneficial effects at later stages of the disease in an APP/PS1 model, where it attenuates deficits in spatial learning and accumulation of amyloid plaques (Zhang et al., 2014). In our pre-symptomatic and pre-plaque model, LTG administration had some common effects in Wt and Tg2576 animals, as well as some different outcomes in the two genotypes. At single cell level, LTG decreased the number of spikes in response to depolarizing steps in both Wt and Tg2576 cells. This effect has been previously shown to be partly dependent on HCN channels (assessed through the sensitivity to the HCN selective blocker ZD7288) and partly independent (Kazmierska-Grebowska et al., 2021). Our results suggest that the decrease in excitability induced by LTG is at least partly attributable to its use-dependent inhibition of Na^+ channels (Kuo and Lu, 1997). This mechanism also likely underlies the LTG-mediated increase in seizure susceptibility observed in both genotypes but not the beneficial effect on memory, since this was observed only in the transgenic group. Of note, previous studies have shown that sodium channel blockers impair cognition both in AD mice (Verret et al., 2012) and in patients with dementia (Cumbo and Ligori, 2010; Mendez and Lim, 2003). In terms of seizure control, sodium channel blockers also had a worse outcome than LTG or levetiracetam in animals (Gureviciene et al., 2019; Sanchez et al., 2012; Verret et al., 2012; Ziyatdinova et al., 2011) and in patients with aMCI or early AD (Vossel et al., 2013).

Among the effects of LTG that were specific to the Tg2576 group, we observed an amelioration of memory performance, as well as a rescue of the I_h sag and resonance properties. The lack of a significant effect of LTG on I_h and resonance in Wt cells is in line with data found by others (Huang et al., 2016; Kazmierska-Grebowska et al., 2021). This can be explained by the fact that, in healthy conditions, HCN channels are predominantly located on distal dendrites (Poolos et al., 2002), while our recordings were made at the somatic level. On the contrary, in the hippocampus of AD transgenic mice, HCN channels are not appropriately trafficked to distal dendrites and are instead sequestered perisomatically, leading to a mixed HCN channellopathy detectable in CA1 pyramidal neurons (Musial et al., 2018). This explains the apparent paradox by which, despite lower expression levels of HCN channels in Tg2576 animals, LTG increases I_h on neurons with this genotype more often than on Wt neurons. HCN mislocalization could also paradoxically lead to the impossibility to detect a difference in the sag recorded at later, intermediate, stages of the pathology.

Since ES intensity was adjusted to match seizure score in the LTG- and the VEH-treated groups, our results demonstrate that LTG prevented seizure-induced memory deficits not by a simple decrease of seizure occurrence. Moreover, LTG did not improve memory in Wt mice, which were also matched for seizure score. This suggests that LTG counteracted the AD-specific deleterious effects of seizures by preventing the network alterations underlying such deficits. Our electrophysiological data point to a rescue of I_h-related properties of CA1 cells, but the biochemical mechanisms involving HCN channels were not investigated. One possibility is through the modulation of oligomeric Aβ. Our findings confirmed that seizures increase extracellular Aβ levels in AD mice (Cirrito et al., 2005; Kamenetz et al., 2003) and further provided evidence that this increase concerns OC-positive fibrillar species. This type of fibrils have been demonstrated to accumulate with age (Liu et al., 2015) and to lead to reduced memory capacity (De Risi et al., 2020). Thus, our results indicate that seizures promote the production of toxic oligomeric fibrillar Aβ at pre-symptomatic stages.

Several pieces of evidence point to a possible link between increased Aβ production and lower HCN expression. The simplest interpretation of our data would be that lower HCN levels lead to increased neuronal excitability that in turn induces extracellular Aβ accumulation (Cirrito et al., 2005; Kamenetz et al., 2003; Minkeviciene et al., 2009). Thus, simply restoring neuronal excitability with LTG prevents aberrant modulation of extracellular Aβ, possibly by reducing β-secretase cleavage of APP (Kamenetz et al., 2003; Zhang et al., 2014). However, in our experiments LTG prevented Aβ accumulation in Tg2576 mice even if these were undergoing the same amount of seizures as the VEH-treated group. That is, even when brain networks of LTG- and VEH-treated AD mice were presumably experiencing the same amount of activity, Aβ increased only in the VEH group. This result argues in favor of a specific Aβ-HCN mechanism over, or along with, Aβ produced by generalized increased neuronal activity. The specificity of this interaction is also supported by the fact that administration of another AED, i.e. levetiracetam, to J20 mice does not alter Aβ levels, despite being effective in reducing abnormal EEG activity and in rescuing memory and synaptic deficits at a symptomatic stage (Sanchez et al., 2012). Moreover, HCN1 levels modulate Aβ production and their deletion in mice enhances Aβ generation (Saito et al., 2012). Finally, HCN1 also associate with APP through X11/Mint adaptor proteins, that in turn regulate APP metabolism (Ho et al., 2008; Rogelj et al., 2006; Sullivan et al., 2014).

In order to understand whether the beneficial effect of LTG on cognition might be through HCN channels, we investigated the action of this AED on pyramidal neurons, which exhibit hyperexcitability already at pre-symptomatic stages of the disease. Indeed, LTG has been shown to decrease the excitability of these neurons by producing a depolarizing shift in I_h activation (Poolos et al., 2002). In addition, LTG, by directly binding HCN channels, could disrupt the association between HCN1, APP and X11 (Saito et al., 2012). While our data support a role for pyramidal neuron HCN channels in determining deficits in AD, other cell types might exhibit alterations already at this stage and could be impacted by LTG. Another study (Hijazi et al., 2020) found that hippocampal parvalbumin-positive interneurons, but not pyramidal neurons, exhibit increased hyperexcitability at early stages of the disease. However, different mouse models show different time profiles in terms of cognitive decline and thus presumably of the appearance of the underlying cellular impairments (Randall et al., 2010). This could be due to time and space variability in the accumulation of Aβ, especially in the first stages of the disease, that in turn non-linearly modulates memory and transmission (Puzzo et al., 2008). In addition, alterations in electrophysiological parameters are not linear, possibly due to compensatory effects or, in this specific case, to an interplay between a decrease in HCN channels and their mislocalization (Musial et al., 2018).

The results of this study should be considered in the context of several limitations. First, although HCN1 levels and related electrophysiological alterations (including rescue by LTG) were assessed in both male and female mice, the CFC and Aβ experiments were performed only in male mice. Since the interaction between epilepsy and AD, as well as the mechanisms affecting Aβ production or its impact could be different in the two sexes, future studies will be needed to assess these possible differences. Also, we assessed the impact of our manipulations on $A\beta_{42}$ but not $A\beta_{40}$ oligomers, leaving open the question of how the latter are affected. Finally, we did not assess whether expression levels of HCN1 are altered by LTG. Thus we cannot exclude that this drug, along with increasing activation levels of HCN channels,

also affects HCN expression.

Collectively, our experiments suggest that LTG does not simply act as an anti-convulsive drug, but also functions as a disease-modifying treatment that lowers the detrimental effects of epilepsy during the pre-symptomatic stages of AD. Of note, LTG has been shown to have beneficial effects on mood disorders associated with AD (Cumbo and Ligori, 2010). Thus, our data provide a rationale to repurpose LTG in the context of pre-symptomatic AD treatment (Vossel et al., 2013).

5. Conclusions

Epilepsy is a comorbidity associated with AD, often starting many years earlier than memory decline. Our study provides evidence of hippocampal neuronal alterations related to lower HCN protein levels in the pre-symptomatic stages of the disease. These alterations are associated with neuronal hyperexcitability, higher susceptibility to seizures and to AD-specific, seizure-induced, memory impairment. Our findings also provide a basis for the use of the antiepileptic drug lamotrigine to counteract acceleration of AD in the early phases of the pathology.

Supplementary data to this article can be found online at https://doi.org/10.1016/j.nbd.2023.106106.

Funding

This work was supported by the American Alzheimer's Association, NIRG-12-237009, awarded to C.M, and by Fondo Ordinario Enti (FOE D. M. 865/2019) funds, in the framework of a collaboration agreement between the Italian National Research Council and EBRI (2019–2021). G.C. received funds from the Fondo di Ateneo per la Ricerca (FAR 2016) Unimore. Funding bodies had no role in the design of the study or in the collection, analysis, and interpretation of data.

Authors' contributions

C.M. conceived all parts of the study. C.M., S.M., G.C. designed the behavioral experiments. E.R., D.P. and G.P. performed electrophysiological experiments. S.M., D.P. G.T. and M.S. performed *in vivo* experiments. F.M., E.M. and A.P. performed Aβ protein extractions for immunoblots, carried out by A.P. Western blot experiments on HCN channels were performed by C.P. and C.G. All authors read and approved the final manuscript.

Declaration of Competing Interest

G.C. has received consulting fees from PassageBio unrelated to this Project.

Data availability

The data that support the findings of this study are available from the corresponding authors, upon reasonable request.

Acknowledgements

We wish to thank Dr. Giovanni Meli and Dr. Annalisa Manca for valuable indications on the Aβ experiments, Prof. Cherubini for helpful discussions on an earlier draft of the manuscript, Dr. Brijesh Modi for contributing to validate our ZAP analysis and Zahra Hemmat for help with the videorecordings.

References

Alcantara-Gonzalez, D., Chartampila, E., Criscuolo, C., Scharfman, H.E., 2021. Early changes in synaptic and intrinsic properties of dentate gyrus granule cells in a mouse model of Alzheimer's disease neuropathology and atypical effects of the cholinergic antagonist atropine. Neurobiol. Dis. 152, 105274 https://doi.org/10.1016/j.nbd.2021.105274.

Ascoli, G.A., Gasparini, S., Medinilla, V., Migliore, M., 2010. Local control of postinhibitory rebound spiking in CA1 pyramidal neuron dendrites. J. Neurosci. 30, 6434–6442. https://doi.org/10.1523/JNEUROSCI.4066-09.2010.

Baker, J., Libretto, T., Henley, W., Zeman, A., 2019. A longitudinal study of epileptic seizures in Alzheimer's disease. Front. Neurol. 10, 1266. https://doi.org/10.3389/fneur.2019.01266.

Bakker, A., Krauss, G.L., Albert, M.S., Speck, C.L., Jones, L.R., Stark, C.E., Yassa, M.A., Bassett, S.S., Shelton, A.L., Gallagher, M., 2012. Reduction of hippocampal hyperactivity improves cognition in amnestic mild cognitive impairment. Neuron 74, 467–474. https://doi.org/10.1016/j.neuron.2012.03.023.

Bezzina, C., Verret, L., Juan, C., Remaud, J., Halley, H., Rampon, C., Dahan, L., 2015. Early onset of hypersynchronous network activity and expression of a marker of chronic seizures in the Tg2576 mouse model of Alzheimer's disease. PLoS One 10, 1–14. https://doi.org/10.1371/journal.pone.0119910.

Born, H.A., Kim, J.Y., Savjani, R.R., Das, P., Dabaghian, Y.A., Guo, Q., Yoo, J.W., Schuler, D.R., Cirrito, J.R., Zheng, H., Golde, T.E., Noebels, J.L., Jankowsky, J.L., 2014. Genetic suppression of transgenic APP rescues hypersynchronous network activity in a mouse model of Alzeimer's disease. J. Neurosci. 34, 3826–3840. https://doi.org/10.1523/JNEUROSCI.5171-13.2014.

Brown, J.T., Chin, J., Leiser, S.C., Pangalos, M.N., Randall, A.D., 2011. Altered intrinsic neuronal excitability and reduced Na+ currents in a mouse model of Alzheimer's disease. Neurobiol. Aging 32, 2109.e1–2109.e14. https://doi.org/10.1016/j.neurobiolaging.2011.05.025.

Buzsáki, G., 2002. Theta oscillations in the hippocampus. Neuron 33, 325–340. https://doi.org/10.1016/S0896-6273(02)00586-X.

Buzsáki, G., Moser, E.I., 2013. Memory, navigation and theta rhythm in the hippocampal-entorhinal system. Nat. Neurosci. 16, 130–138. https://doi.org/10.1038/nn.3304.

Cardoso, A., Carvalho, L.S., Lukoyanova, E.A., Lukoyanov, N.V., 2009. Effects of repeated electroconvulsive shock seizures and pilocarpine-induced status epilepticus on emotional behavior in the rat. Epilepsy Behav. 14, 293–299. https://doi.org/10.1016/j.yebeh.2008.11.004.

Castel-Branco, M.M., Alves, G.L., Figueiredo, I.V., Falcão, A.C., Caramona, M.M., 2009. The maximal electroshock seizure (MES) model in the preclinical assessment of potential new antiepileptic drugs. Methods Find. Exp. Clin. Pharmacol. 31, 101–106. https://doi.org/10.1358/mf.2009.31.2.1338414.

Chang, X., Wang, J., Jiang, H., Shi, L., Xie, J., 2019. Hyperpolarization-activated cyclic nucleotide-gated channels: an emerging role in neurodegenerative diseases. Front. Mol. Neurosci. 12, 141. https://doi.org/10.3389/fnmol.2019.00141.

Chawla, M.K., Penner, M.R., Olson, K.M., Sutherland, V.L., Mittelman-Smith, M.A., Barnes, C.A., 2013. Spatial behavior and seizure-induced changes in c-fos mRNA expression in young and old rats. Neurobiol. Aging 34, 1184–1198. https://doi.org/10.1016/j.neurobiolaging.2012.10.017.

Cirrito, J.R., Yamada, K.A., Finn, M.B., Sloviter, R.S., Bales, K.R., May, P.C., Schoepp, D. D., Paul, S.M., Mennerick, S., Holtzman, D.M., 2005. Synaptic activity regulates interstitial fluid amyloid-β levels in vivo. Neuron 48, 913–922. https://doi.org/10.1016/j.neuron.2005.10.028.

Cumbo, E., Ligori, L.D., 2010. Levetiracetam, lamotrigine, and phenobarbital in patients with epileptic seizures and Alzheimer's disease. Epilepsy Behav. 17, 461–466. https://doi.org/10.1016/j.yebeh.2010.01.015.

D'Amelio, M., Cavallucci, V., Middei, S., Marchetti, C., Pacioni, S., Ferri, A., Diamantini, A., De Zio, D., Carrara, P., Battistini, L., Moreno, S., Bacci, A., Ammassari-Teule, M., Marie, H., Cecconi, F., 2011. Caspase-3 triggers early synaptic dysfunction in a mouse model of Alzheimer's disease. Nat. Neurosci. 14, 69–76. https://doi.org/10.1038/nn.2709.

De Risi, M., Torromino, G., Tufano, M., Moriceau, S., Pignataro, A., Rivagorda, M., Carrano, N., Middei, S., Settembre, C., Ammassari-Teule, M., Gardoni, F., Mele, A., Oury, F., De Leonibus, E., 2020. Mechanisms by which autophagy regulates memory capacity in ageing. Aging Cell 19. https://doi.org/10.1111/acel.13189.

Filippini, N., MacIntosh, B.J., Hough, M.G., Goodwin, G.M., Frisoni, G.B., Smith, S.M., Matthews, P.M., Beckmann, C.F., Mackay, C.E., 2009. Distinct patterns of brain activity in young carriers of the APOE-ε4 allele. Proc. Natl. Acad. Sci. U. S. A. 106, 7209–7214. https://doi.org/10.1073/pnas.0811879106.

Giorgi, F.S., Saccaro, L.F., Busceti, C.L., Biagioni, F., Fornai, F., 2020. Epilepsy and Alzheimer's disease: potential mechanisms for an association. Brain Res. Bull. 160, 107–120. https://doi.org/10.1016/j.brainresbull.2020.04.009.

Gu, N., Vervaeke, K., Hu, H., Storm, J.F., 2005. Kv7/KCNQ/M and HCN/h, but not KCa2/SK channels, contribute to the somatic medium after-hyperpolarization and excitability control in CA1 hippocampal pyramidal cells. J. Physiol. 566, 689–715. https://doi.org/10.1113/jphysiol.2005.086835.

Gureviciene, I., Ishchenko, I., Ziyatdinova, S., Jin, N., Lipponen, A., Gurevicius, K., Tanila, H., 2019. Characterization of epileptic spiking associated with brain amyloidosis in APP/PS1 mice. Front. Neurol. 10, 1151. https://doi.org/10.3389/fneur.2019.01151.

Haytural, H., Benfeitas, R., Schedin-Weiss, S., Bereczki, E., Rezeli, M., Unwin, R.D., Wang, X., Dammer, E.B., Johnson, E.C.B., Seyfried, N.T., Winblad, B., Tijms, B.M., Visser, P.J., Frykman, S., Tjernberg, L.O., 2021. Insights into the changes in the proteome of Alzheimer disease elucidated by a meta-analysis. Sci. Data 8. https://doi.org/10.1038/s41597-021-01090-8.

He, C., Chen, F., Li, B., Hu, Z., 2014. Neurophysiology of HCN channels: from cellular functions to multiple regulations. Prog. Neurobiol. https://doi.org/10.1016/j.pneurobio.2013.10.001.

Hijazi, S., Heistek, T.S., Scheltens, P., Neumann, U., Shimshek, D.R., Mansvelder, H.D., Smit, A.B., van Kesteren, R.E., 2020. Early restoration of parvalbumin interneuron activity prevents memory loss and network hyperexcitability in a mouse model of

Alzheimer's disease. Mol. Psychiatry 25, 3380–3398. https://doi.org/10.1038/s41380-019-0483-4.
Ho, A., Liu, X., Südhof, T.C., 2008. Deletion of mint proteins decreases amyloid production in transgenic mouse models of Alzheimer's disease. J. Neurosci. 28, 14392–14400. https://doi.org/10.1523/JNEUROSCI.2481-08.2008.
Hsiao, K., Chapman, P., Nilsen, S., Eckman, C., Harigaya, Y., Younkin, S., Yang, F., Cole, G., 1996. Correlative memory deficits, Aβ elevation, and amyloid plaques in transgenic mice. Science 274, 99–103. https://doi.org/10.1126/science.274.5284.99.
Hu, H., Vervaeke, K., Storm, J.F., 2002. Two forms of electrical resonance at theta frequencies, generated by M-current, h-current and persistent Na+ current in rat hippocampal pyramidal cells. J. Physiol. 545, 783–805. https://doi.org/10.1113/jphysiol.2002.029249.
Hu, H., Vervaeke, K., Graham, L.J., Storm, J.F., 2009. Complementary theta resonance filtering by two spatially segregated mechanisms in CA1 hippocampal pyramidal neurons. J. Neurosci. 29, 14472–14483. https://doi.org/10.1523/JNEUROSCI.0187-09.2009.
Huang, Z., Walker, M.C., Shah, M.M., 2009. Loss of dendritic HCN1 subunits enhances cortical excitability and epileptogenesis. J. Neurosci. 29, 10979–10988. https://doi.org/10.1523/JNEUROSCI.1531-09.2009.
Huang, Y.Y., Liu, Y.C., Lee, C.T., Lin, Y.C., Wang, M.L., Yang, Y.P., Chang, K.Y., Chiou, S. H., 2016. Revisiting the lamotrigine-mediated effect on hippocampal GABAergic transmission. Int. J. Mol. Sci. 17 https://doi.org/10.3390/ijms17071191.
Hutcheon, B., Yarom, Y., 2000. Resonance, oscillation and the intrinsic frequency preferences of neurons. Trends Neurosci. 23, 216–222.
Irizarry, M.C., Jin, S., He, F., Emond, J.A., Raman, R., Thomas, R.G., Sano, M., Quinn, J. F., Tariot, P.N., Galasko, D.R., Ishihara, L.S., Weil, J.G., Aisen, P.S., 2012. Incidence of new-onset seizures in mild to moderate Alzheimer disease. Arch. Neurol. 69, 368–372. https://doi.org/10.1001/archneurol.2011.830.
Jansson, L., Wennström, M., Johanson, A., Tingström, A., 2009. Glial cell activation in response to electroconvulsive seizures. Prog. Neuro-Psychopharmacol. Biol. Psychiatry 33, 1119–1128. https://doi.org/10.1016/j.pnpbp.2009.06.007.
Kam, K., Duffy, Á.M., Moretto, J., LaFrancois, J.J., Scharfman, H.E., 2016. Interictal spikes during sleep are an early defect in the Tg2576 mouse model of β-amyloid neuropathology. Sci. Rep. https://doi.org/10.1038/srep20119.
Kamenetz, F., Tomita, T., Hsieh, H., Seabrook, G., Borchelt, D., Iwatsubo, T., Sisodia, S., Malinow, R., 2003. APP processing and synaptic function. Neuron 37, 925–937. https://doi.org/10.1016/S0896-6273(03)00124-7.
Kayed, R., Head, E., Sarsoza, F., Saing, T., Cotman, C.W., Necula, M., Margol, L., Wu, J., Breydo, L., Thompson, J.L., Rasool, S., Gurlo, T., Butler, P., Glabe, C.G., 2007. Fibril specific, conformation dependent antibodies recognize a generic epitope common to amyloid fibrils and fibrillar oligomers that is absent in prefibrillar oligomers. Mol. Neurodegener. 2, 1–11. https://doi.org/10.1186/1750-1326-2-18.
Kazim, S.F., Seo, J.H., Bianchi, R., Larson, C.S., Sharma, A., Wong, R.K.S., Gorbachev, K. Y., Pereira, A.C., 2021. Neuronal network excitability in Alzheimer's disease: the puzzle of similar versus divergent roles of amyloid B and TAU. eNeuro. https://doi.org/10.1523/ENEURO.0418-20.2020.
Kazmierska-Grebowska, P., Siwiec, M., Sowa, J.E., Caban, B., Kowalczyk, T., Bocian, R., Maciver, M.B., 2021. Lamotrigine attenuates neuronal excitability, depresses GABA synaptic inhibition, and modulates theta rhythms in rat hippocampus. Int. J. Mol. Sci. 22 https://doi.org/10.3390/ijms222413604.
Kerrigan, T.L., Brown, J.T., Randall, A.D., 2014. Characterization of altered intrinsic excitability in hippocampal CA1 pyramidal cells of the Aβ-overproducing PDAPP mouse. Neuropharmacology 79, 515–524. https://doi.org/10.1016/j.neuropharm.2013.09.004.
Khaliq, Z.M., Bean, B.P., 2010. Pacemaking in dopaminergic ventral tegmental area neurons: depolarizing drive from background and voltage-dependent sodium conductances. J. Neurosci. 30, 7401–7413. https://doi.org/10.1523/JNEUROSCI.0143-10.2010.
Kim, K.R., Kim, Yoonsub, Jeong, H.J., Kang, J.S., Lee, Sang Hun, Kim, Yujin, Lee, Suk Ho, Ho, W.K., 2021. Impaired pattern separation in Tg2576 mice is associated with hyperexcitable dentate gyrus caused by Kv4.1 downregulation. Mol. Brain 14, 62. https://doi.org/10.1186/s13041-021-00774-x.
Kragel, J.E., Vanhaerents, S., Templer, J.W., Schuele, S., Rosenow, J.M., Nilakantan, A. S., Bridge, D.J., 2020. Hippocampal theta coordinates memory processing during visual exploration. Elife 9. https://doi.org/10.7554/eLife.52108.
Kuo, C.C., Lu, L., 1997. Characterization of lamotrigine inhibition of Na+ channels in rat hippocampal neurones. Br. J. Pharmacol. 121, 1231–1238. https://doi.org/10.1038/sj.bjp.0701221.
Li, Chang jun, Lu, Y., Zhou, M., Zong, X. gang, Li, Cai, Xu, X. lin, Guo, L.jun, Lu, Q., 2014. Activation of GABAB receptors ameliorates cognitive impairment via restoring the balance of HCN1/HCN2 surface expression in the hippocampal CA1 area in rats with chronic cerebral hypoperfusion. Mol. Neurobiol. 50, 704–720. https://doi.org/10.1007/s12035-014-8736-3.
Liu, P., Reed, M.N., Kotilinek, L.A., Grant, M.K.O., Forster, C.L., Qiang, W., Shapiro, S.L., Reichl, J.H., Chiang, A.C.A., Jankowsky, J.L., Wilmot, C.M., Cleary, J.P., Zahs, K.R., Ashe, K.H., 2015. Quaternary structure defines a large class of amyloid-β oligomers neutralized by sequestration. Cell Rep. 11, 1760–1771. https://doi.org/10.1016/j.celrep.2015.05.021.
Luo, P., Lu, Y., Li, C., Zhou, M., Chen, C., Lu, Q., Xu, X., He, Z., Guo, L., 2015. Long-lasting spatial learning and memory impairments caused by chronic cerebral hypoperfusion associate with a dynamic change of HCN1/HCN2 expression in hippocampal CA1 region. Neurobiol. Learn. Mem. 123, 72–83. https://doi.org/10.1016/j.nlm.2015.05.005.
Maren, S., Phan, K.L., Liberzon, I., 2013. The contextual brain: implications for fear conditioning, extinction and psychopathology. Nat. Rev. Neurosci. https://doi.org/10.1038/nrn3492.
Mareš, P., Kubová, H., 2006. Electrical stimulation-induced models of seizures. In: Models of Seizures and Epilepsy. Elsevier Inc, pp. 153–159. https://doi.org/10.1016/B978-012088554-1/50014-1.
Marini, C., Porro, A., Rastetter, A., Dalle, C., Rivolta, I., Bauer, D., Oegema, R., Nava, C., Parrini, E., Mei, D., Mercer, C., Dhamija, R., Chambers, C., Coubes, C., Thévenon, J., Kuentz, P., Julia, S., Pasquier, L., Dubourg, C., Carré, W., Rosati, A., Melani, F., Pisano, T., Giardino, M., Innes, A.M., Alembik, Y., Scheidecker, S., Santos, M., Figueiroa, S., Garrido, C., Fusco, C., Frattini, D., Spagnoli, C., Binda, A., Granata, T., Ragona, F., Freri, E., Franceschetti, S., Canafoglia, L., Castellotti, B., Gellera, C., Milanesi, R., Mancardi, M.M., Clark, D.R., Kok, F., Helbig, K.L., Ichikawa, S., Sadler, L., Neupauerová, J., Laššuthova, P., Štěrbová, K., Laridon, A., Brilstra, E., Koeleman, B., Lemke, J.R., Zara, F., Striano, P., Soblet, J., Smits, G., Deconinck, N., Barbuti, A., Difrancesco, D., Leguern, E., Guerrini, R., Santoro, B., Hamacher, K., Thiel, G., Moroni, A., Difrancesco, J.C., Depienne, C., 2018. HCN1 mutation spectrum: from neonatal epileptic encephalopathy to benign generalized epilepsy and beyond. Brain 141, 3160–3178. https://doi.org/10.1093/brain/awy263.
Meli, G., Lecci, A., Manca, A., Krako, N., Albertini, V., Benussi, L., Ghidoni, R., Cattaneo, A., 2014. Conformational targeting of intracellular A' 2 oligomers demonstrates their pathological oligomerization inside the endoplasmic reticulum. Nat. Commun. 5, 3867. https://doi.org/10.1038/ncomms4867.
Mendez, M.F., Lim, G.T.H., 2003. Seizures in elderly patients with dementia: epidemiology and management. Drugs Aging 20, 791–803. https://doi.org/10.2165/00002512-200320110-00001.
Metz, A.E., Spruston, N., Martina, M., 2007. Dendritic D-type potassium currents inhibit the spike afterdepolarization in rat hippocampal CA1 pyramidal neurons. J. Physiol. 581, 175–187. https://doi.org/10.1113/jphysiol.2006.127068.
Minkeviciene, R., Rheims, S., Dobszay, M.B., Zilberter, M., Hartikainen, J., Fülöp, L., Penke, B., Zilberter, Y., Harkany, T., Pitkänen, A., Tanila, H., 2009. Amyloid β-induced neuronal hyperexcitability triggers progressive epilepsy. J. Neurosci. 29, 3453–3462. https://doi.org/10.1523/JNEUROSCI.5215-08.2009.
Moosmang, S., Biel, M., Hofmann, F., Ludwig, A., 1999. Differential distribution of four hyperpolarization-activated cation channels in mouse brain. Biol. Chem. 380, 975–980. https://doi.org/10.1515/BC.1999.121.
Musial, T.F., Molina-Campos, E., Bean, L.A., Ybarra, N., Borenstein, R., Russo, M.L., Buss, E.W., Justus, D., Neuman, K.M., Ayala, G.D., Mullen, S.A., Voskobiynyk, Y., Tulisiak, C.T., Fels, J.A., Corbett, N.J., Carballo, G., Kennedy, C.D., Popovic, J., Ramos-Franco, J., Fill, M., Pergande, M.R., Borgia, J.A., Corbett, G.T., Pahan, K., Han, Y., Chetkovich, D.M., Vassar, R.J., Byrne, R.W., Matthew, Oh.M., Stoub, T.R., Remy, S., Disterhoft, J.F., Nicholson, D.A., 2018. Store depletion-induced h-channel plasticity rescues a channelopathy linked to Alzheimer's disease. Neurobiol. Learn. Mem. 154, 141–157. https://doi.org/10.1016/j.nlm.2018.06.004.
Nolan, M.F., Malleret, G., Dudman, J.T., Buhl, D.L., Santoro, B., Gibbs, E., Vronskaya, S., Buzsáki, G., Siegelbaum, S.A., Kandel, E.R., Morozov, A., 2004. A behavioral role for dendritic integration: HCN1 channels constrain spatial memory and plasticity at inputs to distal dendrites of CA1 pyramidal neurons. Cell 119, 719–732. https://doi.org/10.1016/j.cell.2004.11.020.
Palop, J.J., Mucke, L., 2016. Network abnormalities and interneuron dysfunction in Alzheimer disease. Nat. Rev. Neurosci. 17, 777–792. https://doi.org/10.1038/nrn.2016.141.
Peters, H.C., Hu, H., Pongs, O., Storm, J.F., Isbrandt, D., 2005. Conditional transgenic suppression of M channels in mouse brain reveals functions in neuronal excitability, resonance and behavior. Nat. Neurosci. 8, 51–60. https://doi.org/10.1038/nn1375.
Pignataro, A., Meli, G., Pagano, R., Fontebasso, V., Battistella, R., Conforto, G., Ammassari-Teule, M., Middei, S., 2019. Activity-induced amyloid-β oligomers drive compensatory synaptic rearrangements in brain circuits controlling memory of presymptomatic Alzheimer's disease mice. Biol. Psychiatry 86, 185–195. https://doi.org/10.1016/j.biopsych.2018.10.018.
Poolos, N.P., Migliore, M., Johnston, D., 2002. Pharmacological upregulation of h-channels reduces the excitability of pyramidal neuron dendrites. Nat. Neurosci. 5, 767–774. https://doi.org/10.1038/nn891.
Puzzo, D., Privitera, L., Leznik, E., Fà, M., Staniszewski, A., Palmeri, A., Arancio, O., 2008. Picomolar amyloid-β positively modulates synaptic plasticity and memory in hippocampus. J. Neurosci. 28, 14537–14545. https://doi.org/10.1523/JNEUROSCI.2692-08.2008.
Racine, R.J., 1972. Modification of seizure activity by electrical stimulation: II. Motor seizure. Electroencephalogr. Clin. Neurophysiol. 32, 281–294. https://doi.org/10.1016/0013-4694(72)90177-0.
Randall, A.D., Witton, J., Booth, C., Hynes-Allen, A., Brown, J.T., 2010. The functional neurophysiology of the amyloid precursor protein (APP) processing pathway. Neuropharmacology. https://doi.org/10.1016/j.neuropharm.2010.02.011.
Rizzello, E., Middei, S., Marchetti, C., 2020. Synaptic correlates of anterograde amnesia and intact retrograde memory in a mouse model of Alzheimer's disease. Curr. Alzheimer Res. 17, 259–268. https://doi.org/10.2174/1567205017666200224122113.
Rogelj, B., Mitchell, J.C., Miller, C.C.J., McLoughlin, D.M., 2006. The X11/mint family of adaptor proteins. Brain Res. Rev. 52, 305–315. https://doi.org/10.1016/j.brainresrev.2006.04.005.
Saito, Y., Inoue, T., Zhu, G., Kimura, Naoki, Okada, M., Nishimura, M., Kimura, Nobuyuki, Murayama, S., Kaneko, S., Shigemoto, R., Imoto, K., Suzuki, T., 2012. Hyperpolarization-activated cyclic nucleotide gated channels: a potential molecular link between epileptic seizures and Aβ generation in Alzheimer's disease. Mol. Neurodegener. 7, 1. https://doi.org/10.1186/1750-1326-7-50.

Sanchez, P.E., Zhu, L., Verret, L., Vossel, K.A., Orr, A.G., Cirrito, J.R., Devidze, N., Ho, K., Yu, G.Q., Palop, J.J., Mucke, L., 2012. Levetiracetam suppresses neuronal network dysfunction and reverses synaptic and cognitive deficits in an Alzheimer's disease model. Proc. Natl. Acad. Sci. U. S. A. 109 https://doi.org/10.1073/pnas.1121081109.

Šišková, Z., Justus, D., Kaneko, H., Friedrichs, D., Henneberg, N., Beutel, T., Pitsch, J., Schoch, S., Becker, A., von der Kammer, H., Remy, S., 2014. Dendritic structural degeneration is functionally linked to cellular hyperexcitability in a mouse model of Alzheimer's disease. Neuron 84, 1023–1033. https://doi.org/10.1016/j.neuron.2014.10.024.

Sullivan, S.E., Dillon, G.M., Sullivan, J.M., Ho, A., 2014. Mint proteins are required for synaptic activity-dependent amyloid precursor protein (APP) trafficking and amyloid β generation. J. Biol. Chem. 289, 15374–15383. https://doi.org/10.1074/jbc.M113.541003.

Szabo, A., Cattaud, V., Bezzina, C., Dard, R.F., Sayegh, F., Gauzin, S., Lejards, C., Valton, L., Rampon, C., Verret, L., Dahan, L., 2023. Neuronal hyperexcitability in the Tg2576 mouse model of Alzheimer's disease – the influence of sleep and noradrenergic transmission. Neurobiol. Aging 123, 35–48. https://doi.org/10.1016/j.neurobiolaging.2022.11.017.

Tamagnini, F., Novelia, J., Kerrigan, T.L., Brown, J.T., Tsaneva-Atanasova, K., Randall, A.D., 2015. Altered intrinsic excitability of hippocampal CA1 pyramidal neurons in aged PDAPP mice. Front. Cell. Neurosci. 9, 372. https://doi.org/10.3389/fncel.2015.00372.

Toniolo, S., Sen, A., Husain, M., 2020. Modulation of brain hyperexcitability: potential new therapeutic approaches in Alzheimer's disease. Int. J. Mol. Sci. 21, 1–37. https://doi.org/10.3390/ijms21239318.

Verret, L., Mann, E.O., Hang, G.B., Barth, A.M.I., Cobos, I., Ho, K., Devidze, N., Masliah, E., Kreitzer, A.C., Mody, I., Mucke, L., Palop, J.J., 2012. Inhibitory interneuron deficit links altered network activity and cognitive dysfunction in Alzheimer model. Cell 149, 708–721. https://doi.org/10.1016/j.cell.2012.02.046.

Vossel, K.A., Beagle, A.J., Rabinovici, G.D., Shu, H., Lee, S.E., Naasan, G., Hegde, M., Cornes, S.B., Henry, M.L., Nelson, A.B., Seeley, W.W., Geschwind, M.D., Gorno-Tempini, M.L., Shih, T., Kirsch, H.E., Garcia, P.A., Miller, B.L., Mucke, L., 2013. Seizures and epileptiform activity in the early stages of Alzheimer disease. JAMA Neurol. 70, 1158–1166. https://doi.org/10.1001/jamaneurol.2013.136.

Vossel, K.A., Ranasinghe, K.G., Beagle, A.J., Mizuiri, D., Honma, S.M., Dowling, A.F., Darwish, S.M., Van Berlo, V., Barnes, D.E., Mantle, M., Karydas, A.M., Coppola, G., Roberson, E.D., Miller, B.L., Garcia, P.A., Kirsch, H.E., Mucke, L., Nagarajan, S.S., 2016. Incidence and impact of subclinical epileptiform activity in Alzheimer's disease. Ann. Neurol. 80, 858–870. https://doi.org/10.1002/ana.24794.

Vossel, K.A., Tartaglia, M.C., Nygaard, H.B., Zeman, A.Z., Miller, B.L., 2017. Epileptic activity in Alzheimer's disease: causes and clinical relevance. Lancet Neurol. 16, 311–322. https://doi.org/10.1016/S1474-4422(17)30044-3.

Westmark, C.J., 2013. What's hAPPening at synapses the role of amyloid β-protein precursor and β-amyloid in neurological disorders. Mol. Psychiatry. https://doi.org/10.1038/mp.2012.122.

Westmark, C.J., Westmark, P.R., Malter, J.S., 2010. Alzheimer's disease and down syndrome rodent models exhibit audiogenic seizures. J. Alzheimers Dis. 20, 1009–1013. https://doi.org/10.3233/JAD-2010-100087.

Wykes, R., Kalmbach, A., Eliava, M., Waters, J., 2012. Changes in the physiology of CA1 hippocampal pyramidal neurons in preplaque CRND8 mice. Neurobiol. Aging 33, 1609–1623. https://doi.org/10.1016/j.neurobiolaging.2011.05.001.

Zhang, M.Y., Zheng, C.Y., Zou, M.M., Zhu, J.W., Zhang, Y., Wang, J., Liu, C.F., Li, Q.F., Xiao, Z.C., Li, S., Ma, Q.H., Xu, R.X., 2014. Lamotrigine attenuates deficits in synaptic plasticity and accumulation of amyloid plaques in APP/PS1 transgenic mice. Neurobiol. Aging 35, 2713–2725. https://doi.org/10.1016/j.neurobiolaging.2014.06.009.

Ziyatdinova, S., Gurevicius, K., Kutchiashvili, N., Bolkvadze, T., Nissinen, J., Tanila, H., Pitkänen, A., 2011. Spontaneous epileptiform discharges in a mouse model of Alzheimer's disease are suppressed by antiepileptic drugs that block sodium channels. Epilepsy Res. 94, 75–85. https://doi.org/10.1016/j.eplepsyres.2011.01.003.